Synthetic lethal targeting of oncogenic transcription factors in acute myeloid leukemia using PARP inhibitors

Maria Teresa Esposito[1], Lu Zhao[1], Tsz Kan Fung[1], Jayant K. Rane[1], Amanda Wilson[1], Nadine Martin[2,3], Jesus Gil[2], Anskar Y. Leung[4], Alan Ashworth[5,6], and Chi Wai Eric So[1]

[1] Leukemia and Stem Cell Biology Group. Department of Haematological Medicine, King's College London, Denmark Hill campus SE5 9NU, London UK

[2] Cell Proliferation Group. Medical Research Council Clinical Sciences Centre, Imperial College London, Hammersmith Campus, London W12 0NN, UK

[3] current address: Senescence escape mechanisms lab, Centre de Recherche en Cancérologie de Lyon, Inserm U1052, CNRS UMR5286, F-69000 Lyon, France

[4] Department of Medicine, The University of Hong Kong, Hong Kong, China

[5] The Institute of Cancer Research, Fulham Road, Chelsea, SW3 6JB, UK

[6] current address: UCSF Helen Diller Family Comprehensive Cancer Center, 1450 3rd Street, San Francisco, California, 94158, US

Corresponding author: eric.so@kcl.ac.uk

Abstract

Acute myeloid leukemia (AML) is mostly driven by oncogenic transcription factors, which have been classically viewed as intractable targets using small molecule inhibitor approaches. Here, we demonstrate that AML driven by repressive transcription factors including AML1-ETO and PML-RARα are extremely sensitive to Poly (ADP-ribose) Polymerase (PARP) inhibitor (PARPi), in part due to their suppressed expression of key homologous recombination genes and thus compromised DNA damage response (DDR). In contrast, leukemia driven by MLL fusions with dominant transactivation ability is proficient in DDR and insensitive to PARP inhibition. Intriguing, depletion of an MLL downstream target, Hoxa9 that activates expression of various HR genes, impairs DDR and sensitizes MLL leukemia to PARPi. Conversely, Hoxa9 over-expression confers PARPi resistance to AML1-ETO and PML-RARα transformed cells. Together, these

studies describe a potential utility of PARPi-induced synthetic lethality for leukemia treatment and reveal a novel molecular mechanism governing PARPi sensitivity in AML.

Keywords: PARP, PARPi, AML, leukemia, AML1-ETO, PML-RARα, MLL leukemia, Hoxa9, DNA damage, DNA repair, DDR, synthetic lethality

Introduction

Since its application in *BRCA1/2* mutated cancer in just a decade ago, synthetic lethal approaches induced by Poly-(ADP-ribose)-polymerase (PARP) inhibitors (PARPi) have given renewed enthusiasm to developing anticancer treatments that can specifically target cancer cells but spare the normal[1,2]. While different models have been proposed to explain the molecular mechanisms underlying the synthetic lethality[3,4], they mostly attribute to the critical function of PARP in a variety of DNA repair processes including Base Excision Repair (BER) as a critical sensor of Single Strand Breaks (SSBs)[5,6], Homologous Recombination (HR) as a mediator for restart of stalled replication forks of HR-mediated Double Strand Break (DSB) repair[7-9], and Non-Homologous End-Joining pathway (NHEJ) by preventing the binding of Ku proteins to DNA ends[10]. Specifically, inhibition of BER impairs SSB repair, which results in accumulation of DSB at the replication forks during the S-phase. While it is also noted that an alternative but not mutative exclusive model has also been proposed where PARPi may actually function as poisons that result in PARP trapping[4], DNA repair and survival of PARP inhibited cells seem to be heavily dependent of HR, which are compromised in cancer cells carrying BRCA related mutations[11-17] leading to their unique susceptibility to PARPi treatment.

In spite of the promise in breast and ovarian cancer, clinical application of PARPi has not widely been translated to different cancers as an effective treatment since mutations affecting DNA Damage Response (DDR) genes are not common in other malignancies including acute myeloid leukemia (AML)[18], which is mainly driven by mutated transcription factors such as AML1-ETO, PML-RARα and MLL fusions[19]. Despite the advance in understanding of the genetic basis of the disease, the same chemotherapy treatment developed over half a century ago are still used for all AML patients, the only exception being Acute Promyelocytic Leukemia (APL) carrying PML-

RARα[20]. Due to the high general toxicity, chemotherapy can usually only apply to young patients of age under 60, leaving little or no treatment options for the majority of AML patients. In addition, standard chemotherapy only induces long-term complete remission in less than 40% of patients and is mostly ineffective in patients carrying mutations in the *Mixed Lineage Leukemia* (*MLL*) gene[20]. Therefore there is an urgent need to develop better therapeutic strategies for AML.

Since specific transcriptional programs including those involved in DDR are frequently deregulated by various oncogenic transcription factors, we reasoned that transcriptional deregulation might represent an alternative mechanism allowing the targets of differential DDR for effective leukemia treatments[18]. To this end, we performed extensive molecular and functional analyses of the effect of PARP inhibition on some of the most common forms of AML. Here we show that AML driven by AML1-ETO and PML-RARα, which suppress the expression of DDR genes, exhibit a BRCAness phenotype and can be efficiently targeted by PARPi treatment. On the other hand, MLL-driven leukemia is resistant to PARPi but can be sensitized to the treatment by genetic or pharmacological inhibition of its downstream target, Hoxa9, which mediates effective DDR.

Results

Pharmacological inhibition of PARP selectively suppresses AML1-ETO and PML-RARα mediated leukemia

To explore the therapeutic potentials of targeting PARP in acute leukemia, we investigated the effect of Olaparib, one of the most commonly used clinical PARPi, on clonogenic growth of primary murine hematopoietic cells transformed by the most common leukemia associated transcription factors (LATFs) including AML1-ETO, PML-RARα, MLL-AF9 and E2A-PBX using the retroviral transduction/transformation assay (RTTA), which has been successfully employed to model the corresponding human diseases[21-24]. While a dose-response titration assay identified the *in vitro* maximal tolerable dose at a concentration of up to 1uM Olaparib that exhibited undetectable/minimal effects on normal primary bone marrow cells (Supplementary Fig.

1a-b), the same treatment had striking impacts on primary cells transformed. PARPi significantly suppressed colony forming ability of cells transformed by AML1-ETO or PML-RARα (by about 90% $p<0.001$), although it had little impact on MLL-AF9 or E2A-PBX transformed cells (Fig. 1a-b and Supplementary Fig. 1c-d). To confirm the specificity of the drug, we also reported very similar and selective leukemia suppressive effects using a different PARPi, Veliparib (Supplementary Fig. 1e-f), providing an independent validation of the potential therapeutic application of PARPi on these leukemias. In order to further demonstrate PARP1 as the major molecular target for the observed phenotype, two independently validated shRNAs targeting mouse Parp1 (Supplementary Fig. 1g-h) were used to replace PARPi in the RTTA. Consistent with the chemical inhibitor studies, both Parp1-shRNAs significantly suppressed the colony forming ability of cells transformed by AML1-ETO or PML-RARα (45-70%), but only had a modest impact on E2A-PBX and MLL-AF9 transformed cells (Fig. 1c-d and Supplementary Fig. 1i), indicating a specific requirement of PARP in leukemic cells transformed by AML1-ETO or PML-RARα.

To investigate if PARPi could exert similar inhibitory effects on the corresponding human leukemias, we used patient-derived leukemic cell lines carrying AML1-ETO (Kasumi), mutated PML-RARα that is resistant to standard ATRA treatment (NB4-LR2)[24], or MLL-AF9 (THP1) for the inhibitor studies. Analogous to the observation in the mouse primary transformed cells, PARPi treatment reduced the colony forming ability of Kasumi and NB4-LR2 but did not affect THP1 cells (Fig. 1e-f). To further demonstrate the potential *in vivo* efficacy, Kasumi, NB4-LR2 and THP1 cells were xeno-transplanted into immuno-compromised mice and subjected to the PARPi treatment. In spite of being used as a mono-therapy, Olaparib treatment significantly delayed the disease onset driven by AML1-ETO from median survival of 55 days to 102 days (Fig. 1g, Supplementary Fig. 1j, 1m, and Table S1), providing proof-of-principle evidence for the application of PARPi in AML1-ETO leukemia. Strikingly, Olaparib as a single agent could also effectively suppress disease onset induced by ATRA-resistant APL cells (Fig. 1h, Supplementary Fig. 1k, 1n, and Table S2), highlighting its potential use for treatment-resistant APL[25]. In contrast, PARPi treatment had no effect on the

survival of xenograft model transplanted with human THP1 cells carrying MLL-AF9 (Fig. 1i, Supplementary Fig. 1l, 1o, and Table S3). To further substantiate these findings, we also observed very similar differential *in vitro* PARPi responses using primary AML patient samples carrying the corresponding translocation fusions, in which both AML1-ETO and PML-RARα (but not MLL fusion) primary human leukemia cells were highly sensitive to PARPi (Supplementary Fig. 1p-q). Together, these results reveal the potential therapeutic utility of PARPi in different subtypes of leukemia driven by specific LATFs.

PARPi treatment induces differentiation and senescence

We next investigated the cellular processes being affected by PARPi in primary transformed cells that might explain the inhibitory effect. PARPi treatment on AML1-ETO and PML-RARα transformed cells in clonogenic assay resulted in their morphological differentiation into monocytic/granulocytic lineages (Fig. 2a-b). These results were consistent with the time course measurement of growth and differentiation by both morphology and NBT reduction assays, showing that PARPi could slow cell growth in general but significantly increased the percentage of differentiation only in AML1-ETO and PML-RARα cells (Supplementary Fig. 2a-d). These findings corroborate with recent observations of leukemic differentiation induced by excessive DNA damage[26], suggesting that differential DDR may underlie the contrasting PARPi responses. PARPi treatment was also accompanied by cell cycle G1 arrest (Fig. 2c and Supplementary Fig 2e), up-regulation of p53 and p21 (Fig. 2d-e). Consistently, we also detected an increase of p16 expression in AML1-ETO and PML-RARα transformed cells (Fig. 2f), which underwent significant senescence upon PARPi treatment (Fig. 2g-h). PARPi also induced apoptosis of PML-RARα transformed cells (Fig. 2i and Supplementary Fig. 2f). In contrast, none of these effects were observed in E2A-PBX or MLL-AF9 transformed cells in spite of a small upward trend in differentiation and apoptosis noted in these primary transformed mouse cells upon PARPi treatment (Fig. 2a-i). To further extend our findings to the corresponding human leukemias, similar assays were performed on the human leukemia cell lines and primary human patient samples carrying the translocation fusions. In accord with the results in the mouse

models, PARPi could effectively induce senescence and apoptosis in Kasumi and NB4-LR2 but not THP1 (Supplementary Fig. 2g-i); and increased differentiation of primary AML cells carrying AML1-ETO and PML-RARα but not MLL fusions (Supplementary Fig. 2j-l). These results consistently suggest a specific requirement of PARP function in the leukemic cells transformed by AML1-ETO and PML-RARα.

AML1-ETO and PML-RARα transformed cells show inherent DDR defects

Although the general rationale behind the PARPi sensitivity is a defect in DDR[3,4,15,16,27], PARP also has transcriptional functions involved in gene regulation[1,28]. After the biochemical and transcriptional approaches detected no direct biochemical interaction (Supplementary Fig. 3a and unpublished mass spectrometry data) and transcriptional regulation (Supplementary Fig. 3b-e) between PARP1 and any of these fusion proteins, we assayed DNA damage and the kinetics of the DDR in the primary transformed cells by analyzing the frequency of Ser-139 phosphorylated γ-H2AX foci, which is considered as an early cellular response to DSBs, and the most well established chromatin modification linked to DNA damage and repair[29]. With the exception of E2A-PBX, untreated AML1-ETO, PML-RARα and MLL-AF9 transformed cells displayed significant levels of γH2AX-positive DNA damage foci (with both criteria of >6 and >10 foci), indicative of ongoing DNA damage or replication stress (Fig. 3a-b, Supplementary Fig. 3f). Upon PARPi treatment, both PARPi insensitive (E2A-PBX and MLL-AF9 cells) and sensitive cells (AML1-ETO and PML-RARα) showed further inductions of γH2AX foci (Fig. 3c, Supplementary Fig. 3g-k), suggesting that PARPi treatment induced DNA damage regardless of the onco-fusion proteins expressed by the transformed cells. As PARPi have been demonstrated to selectively target HR deficient cells[3,15,16], we investigated whether PARPi sensitive cells were incapable of effective recruitment of Rad51 to DNA damage sites, as a readout of HR efficiency[30,31]. Upon PARPi treatment for 6 hours, E2A-PBX or MLL-AF9 cells, were able to form RAD51 foci (with both criteria of >6 and >10 foci), which then returned to basal level after the repair in 24 hours (Fig 3c-d, Supplementary Fig. 3g-j,l). In a stark contrast, no significant Rad51 recruitment was observed in AML1-ETO or PML-RARα transformed cells (Fig. 3c-d, Supplementary Fig. 3g-j, l), in which around 80% of the cells showed γH2AX and Rad51

foci ratio greater than 2 (Fig. 3e), indicating their HR deficient nature. The observed differential HR deficiency associated with PARPi treatment cannot be due to different cell cycle status of these cells, as PARPi exhibited no significant effect on cell cycle progression in first 24 hours (Supplementary Fig. 3m) when these assays were performed. To further extend our findings to the human disease, human leukemia cell lines carrying the corresponding fusions were also subjected to similar DDR assays. Consistently, we observed higher levels of DNA damage in untreated Kasumi and NB4-LR2 cells (Supplementary Fig. 3n-o), which also failed to effectively induce Rad51 repair foci upon PARPi treatment as compared with THP1 (Supplementary Fig. 3p-r).

To gain further insights into the differential impacts of LATF on DDR, we investigated the expression of the major HR mediators and revealed a decreased expression of key HR genes including *Rad51*, *Atm*, *Brca1* and *Brca2* in both AML1-ETO and PML-RARα mouse models (Fig. 3f). To validate these findings in the corresponding human leukemias, we analysed the expression array data of these genes in patient samples carrying these distinctive LATFs[32]. Consistently, we observed very similar suppression of a large number of HR mediators in AML1-ETO and PML-RARα human leukemic cells as compared with *MLL* rearranged leukemia (Fig. 3g, Table S4). These results could be independently confirmed by a second set of array data from different patient cohorts[33] (Supplementary Fig. 3s). We also further validated the results of two key HR mediators, RAD51 and BRCA2, at the protein level by Western blot using mouse primary leukemic cells transformed by the corresponding fusions (Fig. 3h), although the differential expression of RAD51 was milder than BRCA2, which were in line with the RNA expression data (Fig. 3f). These results consistently suggest that suppression of HR genes is a distinctive feature shared by PARPi sensitive AML1-ETO and PML-RARα transformed cells. To further assess the direct effect of these fusion proteins on DNA repair efficiency, we performed both plasmid end-joining assay[34] and HR reporter assay[35]. Nuclear extracts from E2A-PBX and MLL-AF9 transformed cells could efficiently repair DSB and produced significantly higher total numbers of colonies as compared to those by AML1-ETO and PML-RARα transformed cells (Fig. 3i). Moreover, in contrast to E2A-PBX and MLL-AF9, most of the end-repairs by AML1-ETO or PML-RARα nuclear extracts were mis-matched (Fig. 3j). Consistently, we also

observed significant suppression of HR efficiency upon expression of AML1-ETO or PML-RARα as opposite to a small notable and significant increase of HR efficiency by MLL-AF9 (Fig. 3k). Therefore these data indicate that leukemic cells driven by AML1-ETO and PML-RARα had a reduced ability to repair DSBs and that the repairs accompanied with an increased error rate, which may form the basis for their increased PARPi sensitivity.

Induction of Hoxa9 expression by MLL fusions modulates PARPi sensitivity

To gain novel mechanistic insights regulating the PARPi sensitivity, we analysed PARPi-resistant MLL leukemic cells, which showed a high basal level of phosphorylated γH2AX (Fig. 3a-b) but were able to efficiently recruit Rad51 to the DNA damage foci (Fig. 3c-d) and survived PARPi treatment (Fig. 1-2), suggesting HR competency. In contrast to AML1-ETO and PML-RARα[19,23], MLL fusion proteins recruit chromatin remodeling enzymes and transactivation complexes culminating in the expression of critical downstream genes, including the homeodomain transcription factor *HOXA9*[19,36,37], which has been previously identified as one of the single most critical independent poor prognostic factors associated with inferior treatment response in AML[38] and its suppression has been linked to the drug resistant phenotype in glioblastoma[39,40]. Consistently, we could observe specific and differential activation of Hoxa9 by MLL fusion in our mouse models and independent human patient data (Supplementary Fig. 4a-c). Thus we hypothesized that the PARPi resistance exhibited by MLL-AF9 transformed cells might be dependent of its ability to activate Hoxa9 expression. To this end, we assessed the functional requirement of Hoxa9 in conferring PARPi resistance in MLL-AF9 transformed cells using RTTA in combined with a *Hoxa9* knockout mouse model. Consistent with the previous report[23,41,42], *Hoxa9* knockout had relatively modest effect on both *in vitro* and *in vivo* transformation mediated by MLL-AF9 its spite of a more mature phenotype and a slightly reduced colony forming ability as compared with their wild type counterpart[41] (Fig. 4a-c and Supplementary Fig. 4d-g). Strikingly, ablation of *Hoxa9* expression sensitized MLL-AF9 transformed cells to PARPi treatment, which resulted in a significant suppression of colony forming ability and differentiation of MLL-AF9 transformed cells (Fig. 4a-c and Supplementary Fig. 4e-f). In contrast, *Hoxa9*

knockout had a modest effect on E2A-PBX transformed cells, which have previousuly been shown as an Hoxa9 independent oncofusion[23,43] (Fig. 4a-c and Supplementary Fig. 4d-e). We also observed induction of senescence in MLL-AF9 *Hoxa9*$^{-/-}$ transformed cells upon PARPi treatment (Fig. 4d-e), which is consistent with the role of Hoxa9 in suppressing cellular senescence[23], a common endpoint of excessive DNA damage. These data indicate that Hoxa9 may play a key role in mediating PARPi resistance in MLL transformed cells, and its suppression in combination with PARPi may represent a novel avenue for targeting MLL leukemia. To this end, we tested the *in vivo* efficacy of this approach using MLL-AF9 full-blown leukemic cells derived from primary transplanted mouse, which closely mimic the advanced clinical stage of the corresponding human disease[22]. As expected, Olaparib treatment did not have any significant effect on mice transplanted with wild type MLL-AF9 leukemic cells (Fig 4f, Supplementary Fig. 4h and Table S5). In contrast, while Hoxa9 deficient MLL-AF9 leukemic cells could efficiently induce leukemia, they were highly sensitive to PARPi treatment, which significantly delayed the disease latency (Fig 4g, Supplementary Fig. 4h and Table S6), indicating a critical function of Hoxa9 in mediating PARPi resistance in MLL leukemia.

To further demonstrate the role of Hoxa9 in mediating PARPi resistance, we also employed a gain of function approach by over-expressing *Hoxa9* in PARPi sensitive AML-ETO and PML-RARα leukemic cells. As expected, AML1-ETO and PML-RARα cells transduced with the vector control remained sensitive to PARPi treatment. Interestingly, forced expression of Hoxa9 conferred PARPi resistant to AML1-ETO and PML-RARα cells without affecting the expression of the fusions (Fig. 4h-j and Supplementary Fig. 4i-j); AML1-ETO or PML-RARα cells co-transduced with Hoxa9 could still form compact colonies with immature myeloblast phenotypes upon PARPi treatment. Hoxa9 expression also suppressed PARPi-induced senescence in AML1-ETO and PML-RARα cells (Fig 4k-l). Together with the loss of function data, these results strongly suggest that Hoxa9 plays a key role in mediating PARPi resistance in leukemic cells.

Hoxa9 activates expression of HR gene expression, promotes Rad51 foci formation and DNA repairs

Given that the primary effect of PARPi treatment is on DNA repair, we analysed the effect of Hoxa9 in mediating DDR in transformed cells. In contrast to AML1-ETO and PML-RARα transformed cells, which were incompetent to mount significant Rad51 repair foci at DNA damage sites upon PARPi treatment (Fig. 3c), Hoxa9 over-expression conferred on these cells the ability to efficiently recruit Rad51 to DNA damage foci (Fig. 5a-b). Over-expression of Hoxa9 had modest effects on E2A-PBX or MLL-AF9 transformed cells, which already showed efficient recruitment of Rad51 (Fig. 5a-b). Conversely, suppression of Hoxa9 expression resulted in a significant impairment of Rad51 recruitment in MLL-AF9 transformed cells (Fig. 5c-d), leading to the hypothesis that Hoxa9 might be an upstream regulator of Rad51. To this end, we analyzed the expression array data of known Hoxa9 downstream targets in primary transformed myeloid cells[44,45]. The gene set enrichment analysis (GSEA) and gene ontology analysis (GO) revealed that genes involved in DNA repair, especially DNA repair with homologous recombination, were significantly enriched in HOXA9 responsive gene set (Fig. 5e, Supplementary Fig. 5a-b, and Table S4). These results were also confirmed by RT-qPCR in *Hoxa9* knockout MLL-AF9 transformed cells (Supplementary Fig.5c). Among them were key HR genes including *Rad51*[12,30,31], which was further validated in the primary transformed cells by both Hoxa9 over-expression (Fig. 5f) and knockout approaches (Fig. 5g). The regulation of RAD51 and BRCA2 expression by Hoxa9 in MLL-AF9 cells were also demonstrated at the protein level, where the expressions of these two proteins were significantly diminished in the absence of Hoxa9 (but not β-catenin control) (Fig. 5h). While these results consistently suggest an important involvement of common HR genes (e.g., Rad51 and Brca2) in mediating differential PARPi responses exhibited by different LATFs, there are also likely other HR targets uniquely regulated by individual LATFs that also contribute to their differential responses. Finally, to demonstrate a direct involvement of HOXA9 in DDR, HR-reporter assays further revealed an enhanced HR efficiency by Hoxa9 expression as opposite to a compromised HR response upon its suppression (Figure 5i). These data strongly suggest that Hoxa9 confers resistance to PARPi in part by activating DDR transcription programs.

Targeting PARPi resistant AML with a combination approach

While there is not yet chemical inhibitor that can directly target Hoxa9, inhibitors are available to target its upstream regulators and essential co-factors, including GSK3, which mediates the phosphorylation of CREB/CBP required for Hox transcriptional functions[46]. We and others have previously shown that GSK3 inhibitor (GSKi) such as LiCl and LiCO3 were effective in suppressing the transcriptional activity of Hox and targeting MLL pre-leukemic stem cells (pre-LSC), but not the advanced stage MLL LSC that acquired resistance in part due to the activation of canonical Wnt/β-catenin pathways and were capable of inducing leukemia with a much shorter latency[22,46,47]. To further explore the potential application of PARPi on MLL leukemia, we assessed the effect of PARPi in combination with GSK3i (LiCl), on both MLL pre-LSC and MLL LSC enriched populations that exhibited contrasting GSKi sensitivity and disease latency[22]. As expected, the application of previously defined optimal concentration of LiCl (Supplementary Fig. 6a)[22,46,47] significantly suppressed the colony forming ability of MLL pre-LSC, but not MLL LSC (Fig. 6a,c, and Supplementary Fig. 6b-c). Interestingly, its combination with otherwise non-effective PARPi treatment led to further increased growth inhibition (Fig. 6a,c), which inversely correlated with transcriptional activity of Hoxa9 as assessed by the expression of its downstream target, *c-myb* (Fig. 6b,d). More strikingly, while individual PARPi or LiCl treatment was ineffective on MLL LSC, their combination dramatically suppressed leukemic cell growth and induced differentiation of MLL LSC (Fig. 6c, e, f). To further demonstrate the *in vivo* efficacy, pretreated MLL LSC were transplanted into syngeneic mice, and subjected to Olaparib, LiCO3, or their combined treatments (Figure 6g). As expected, mice transplanted with control MLL-AF9 cells succumbed to leukemia within 8 weeks (Fig. 6g, Supplementary Fig. 6d-e, and Table S7). PARPi or GSK3i treatment alone did not significantly extend the survival (Fig. 6g, Supplementary Fig. 6d-e, and Table S7). Strikingly, the combined PARPi and GSK3i treatment suppressed leukemia development and all the mice still survived within the 80 days of observation period (Fig. 6g, Supplementary Fig. 6d-e, and Table S7), highlighting the therapeutic potential of the novel combined treatment for MLL leukemia.

To investigate if a similar treatment could also be effective in the corresponding human leukemia, THP1 cells derived from the patient with MLL-AF9 fusion were also tested. As expected, Olaparib alone was ineffective and only modest suppression was observed with LiCl treatment (Supplementary Fig. 6f-g). However in combination, LiCl could sensitize PARPi-resistant THP1 cells to the PARPi treatment resulting in significant growth suppression and differentiation of the leukemic cells (Supplementary Fig. 6f-g). To further strengthen our findings in the relevant clinical setting, we performed the same treatments on two independent primary human patient samples carrying MLL fusions (i.e., patients AML1 and AML2). While limited inhibition was exhibited by individual treatments, their combination showed consistent and significant synergistic effects in suppressing growth and promoting differentiation of both primary MLL leukemic cells (Fig. 6h-k). Finally, to monitor and further demonstrate the *in vivo* treatment efficacy in primary, we labelled the primary MLL leukemic cells from patient AML1 with a luciferase reporter prior their transplantation into NSG mice for drug treatments. By *in vivo* imaging, we observed a rapid disease development as early as 4 weeks post-transplant in the untreated control (Fig. 6l, Supplementary Fig. 6h). A similar rate of disease progression was also observed in cohorts receiving single drug treatments although LiCO3 treated group might exhibit an even faster rate of leukemic growth (Fig. 6l, Supplementary Fig. 6h). In contrast, PARPi/LiCO3 combination treatment significantly prohibited leukemic cell growth *in vivo* (Fig. 6l, Supplementary Fig. 6h). Following the long-term disease development, mice received single drug treatment succumbed to leukemia with a similar phenotype and disease latency as the control group (Fig. 6m, Supplementary Fig. 6i-j, Table S8). Strikingly, the combination treatment significantly suppressed leukemia development and none of the tested subjects succumbed to leukemia throughout the observation period (Fig. 6m, Supplementary Fig. 6i-j). Together, these independent results from mouse models and primary human xenograft models provide the first proof-of-principle pre-clinic evidence for a novel effective therapeutic strategy based on a combined PARPi and GSK3i treatment for MLL leukemia.

Discussion

In spite of the lack of genetic mutations directly affecting DDR genes, we provide molecular evidence and preclinical data showing the potential utility of PARPi-mediated selective killing of leukemic cells carrying specific oncogenic transcription factors (Supplementary Fig. 7). This appears to be due to the differential impacts on these transcription factors on the expression of critical DDR genes involved DDR[48-52]. In addition to the discovery of strong PARPi sensitivity exhibited by AML1-ETO and PML-RARα transformed cells, we also demonstrate for the first time that Hoxa9, an independent poor prognostic factor in AML[38] and a key downstream target of MLL-fusions[53], can activate a potential back-up DDR pathway, which may allow leukemia cells to overcome PARPi. This finding may also in part explain the previously reported S-phase checkpoint dysfunction of MLL-rearranged leukemic cells showing radio-resistant DNA synthesis and chromatid-type genomic abnormalities[54].

Emerging evidence suggests that various Hox proteins may be involved in DNA repair[55,56]. HoxB7 interacts directly with PARP-1 and the complex DNA-PK-Ku80-Ku70 enabling NHEJ pathway[55], whereas HoxB9 promotes HR by inducing TGFβ, which in turn enhances ATM activation and ATM-dependent response in breast cancer cell lines[56]. Our data indicate that Hoxa9 mediates expression of critical DDR genes to stimulate HR and recruitment of Rad51 to DNA damage foci in response to PARPi treatment. Consistent with its putative role in mediating drug resistant in glioma[43,44], we further demonstrate that Hoxa9 over-expression rescues AML1-ETO and PML-RARα cells from PARPi treatment, whereas *Hoxa9* KO makes MLL-AF9 sensitive to PARPi, revealing a novel function of Hoxa9 as a major player in governing PARPi resistance in MLL leukemia.

In line with a classical model of DDR barrier in cancer development[57], a recent study by Takacova et al. demonstrated that inactivation of the DDR barrier through ATM/ATR inhibitors accelerated leukemia driven by a tamoxifen-inducible MLL fusion[58]. On the other hand, Santos et al. have elegantly shown that total genetic ablation of critical DDR genes such as *MLL4, ATM* or *BRCA1*, instead of accelerating, inhibited MLL-driven leukemogenesis by inducing leukemic differentiation[59]. These results suggest dual roles of some of the key DDR players such as ATM in promoting and

suppressing MLL leukemia, which may be dosage and context dependent. Interestingly, Hoxa9 that predominately drives leukemic growth and PARPi resistance is largely dispensable for normal development[23,42,60], highlighting its potential as a therapeutic target. As a proof-of-principle experiment, we further demonstrate that the combined use of PARPi together with the GSK3i that targeted the transcriptional function of Hoxa9[22,46,47] can achieve selective killing of otherwise PARPi-resistant MLL leukemic cells, revealing a potentially novel venue for overcoming PARPi-resistance in leukemia (Supplementary Fig. 7).

Acknowledgements

We thank Ivan Ahel, Ian Gibbs-Seymour, David Livingston for tagged ALPF and PARP1 constructs; Eva Hoffman, Maria Jasin for DR-GFP HR reporter systems; Hyunsook Lee, Madalena Tarsounas for BRCA2 antibody; Jay Hess for MSCV-HA-*Hoxa9*-IRES-GFP construct; Claudio Lourenco and Winston Vetharoy for technical assistance with mice experiments and FACS analysis; Sam Tung, Andrew Innes and Priscilla Lau for technical assistance with gene expression profiling; Terry Gaymes for support with DNA damage repair experiments; Sydney Shall, Tony Ng, Ghulam Mufti, Daniel Weekes for insightful discussion, Pui Tse for graphical illustration. This work was supported by programme grants from Cancer Research UK (CRUK) and Leukaemia and Lymphoma Research (LLR) to CW So.

Materials and Methods

Retroviral Transduction/Transformation Assay (RTTA)

RTTA was performed on primary murine hematopoietic cells as described[21]. c-Kit positive progenitor cells were isolated from wild type Ly5.1 mouse bone marrow, and cultured overnight in R10 medium [RPMI 1640 containing 10% FCS, 100U/mL penicillin and 100μg/mL streptomycin] supplemented with 20ngml^{-1} stem cell factor (SCF), 10ngml^{-1} interleukin (IL)-3, and 10ngml^{-1} IL-6. Transduction using concentrated viral supernatant expressing the oncogene of interest was carried out by centrifugation (spinoculation) at 800*g* at 32 ºC for 2 hours in the presence of 5μg ml^{-1} polybrene

(Sigma-Aldrich). Cells were subsequently plated in 1% methylcellulose medium (M3231; Stem Cell Technologies) containing 20ngml^{-1} SCF, 10ngml^{-1} IL-3, 10ngml^{-1} IL-6 and 10ngml^{-1} granulocyte macrophage colony-stimulating factor (GM–CSF) and appropriate selection antibiotic. Colonies were counted after 7 days of culture and replated every 6-7 days at 5x10^{3}-1.5x10^{4} cell density. Re-plating was performed weekly to generate primary cell lines for further analysis. After the third or fourth round of plating, cells were cultured in R20/20 medium (RPMI 1640, 20% FCS, 20% WEHI-conditioned medium, 2 mM L-glutamine, 100 U/ml penicillin, and 100 μg/ml streptomycin) supplemented with 20ngml^{-1} stem cell factor (SCF), 10ngml^{-1} interleukin (IL)-3, and 10ngml^{-1} IL-6 to establish cell lines. All recombinant murine cytokines were from PeprotechEC.

Cell culture

NB4-LR2 and THP1 cell lines (kindly provided by Dr Arthur Zelent and Professor Mel Greaves respectively) were cultured in RPMI (Invitrogen) supplemented with 10% selected FBS (R10), 2mM L-Glutamine. Kasumi cell line (kindly provided by Dr Olaf Heidenreich) was cultured in RPMI-Hepes modified (Sigma) supplemented with 20% selected FBS and 2mM L-Glutamine (R20). Cell lines were validated by qPCR for their respective oncogenes. NIH3T3 and GP2 cell line was cultured in DMEM (Invitrogen) supplemented with 10% selected FBS and 2mM L-Glutamine. Human primary AML cells were cultured in IMEM (Invitrogen) supplemented with 10% PBS, 2mM L-Glutamine, 10ng/mL each of human cytokines, IL3, IL6, SCF, FLT3 ligand, and TPO. Cells were kept at 37°C and 5%CO_2. Use of human primary cells was approved by King's College London committee and consents of the patients were obtained.

In vitro drug treatment

Most of the inhibitor studies on mouse cells were carried out by plating 3-5x10^{3} cells in 1% methylcellulose medium containing 20ng ml^{-1} SCF, 10ng ml^{-1} IL-3, 10ngml^{-1} IL-6 and 10ng ml^{-1} GM–CSF in the presence of 1μM Olaparib (LC Laboratories), 1μM Veliparib (Abbott) or 8mM Lithium Chloride (LiCl, Sigma) at the concentrations as indicated in the Results section. Colonies were scored 6-7 days after plating. For other *in vitro* studies, mouse leukemic cells and primary AML cell lines were subjected to

continuously Olaparib (1μM) or LiCl (8mM) treatment in liquid culture for whole duration as indicated in the figures or figure legends. For human leukemic cell lines, experiments were performed as described above with 5μM Olaparib.

Flow cytometric analysis

Flow cytometry analyses of mouse leukemic cells for both *in vitro* and *in vivo* experiments were performed as previously described[61] using mouse specific anti-CD11b (Mac-1) (clone M1/70), anti-Gr1 (clone RB6-8C5), anti-c-Kit (clone 2B8), anti-CD45.1 (clone A20) and anti-CD45.2 (clone 104) antibodies from BioLegend. For humanized mouse model, the engrafted human donor cells were analysed using anti-human CD45 (clone H130) and CD33 (clone WM53).

Cell cycle analysis

For each assay $1x10^5$ cells were collected, washed in PBS and fixed in 70% cold ethanol. After re-hydration with PBS and centrifugation at 500g for five minutes, the cells were incubated with a solution of PBS containing 1% FCS, 40ug/ml RNAse and 500ug/ml propidium iodide solution (Sigma-Aldrich) in the dark for 30 minutes at 37° C. Samples were then analyzed at the FACS LSRII (BD Biosciences Pharmingen). DNA peaks were analyzed with FACS Diva.

Annexin V staining

For each assay $1x10^5$ cells were collected, washed in PBS and re-suspended in Annexin V binding solution (25mM Hepes, 140mM KCl, 2.5mM $CaCl_2$ pH 7.2). After centrifugation at 500g for five minutes the cells were incubated with the Annexin V Binding solution containing 0.25 ug/ml mouse anti Annexin V-FITC antibody (Biolegend 640906) and 1ug/ml propidium iodide in the dark for 30 minutes at 4°C. Samples were then washed in PBS analysed at the FACS LSRII (BD Biosciences Pharmingen) with FACS Diva.

Beta galactosidase staining

Cells were cytospun onto a glass slide at 400g for 5 minutes and then fixed for 10 minutes with 2% formaldehyde/0.2% glutaraldehyde (Sigma Aldrich). Cells were then washed with PBS, and then incubated at 37°C for at least 2 hours with a staining solution (30mM Citric Acid/Phosphate buffer, 5mM $K_4Fe(CN)_6$, 5mM $K_3Fe(CN)_6$, 150mM NaCl, 2mM $MgCl_2$, 1mg/ml X-Gal) (All reagents from Sigma-Aldrich)[62]. Cells were counted in at least 5 fields for each slide, for a total of over 100 cells. The percentage of senescent cells was calculated by the percentage of the number of blue cell in the field.

Immunofluorescence staining of γH2AX and RAD51

Cells were cytospun onto a glass slide at 400g for 5 minutes and then fixed for 30 minutes in 4% PFA and permeabilized and blocked in 0.8% Tx-100, 10% FBS/1% BSA (Sigma-Aldrich) in PBS for 15 min at room temperature. Mouse anti mouse γH2AX (ser139) (Upstate clone JBW301 #05-636) and rabbit anti mouse RAD51 (Santa Cruz Biotecnology H92 #sc-8349) were diluted in TBS containing 10%FBS/1%BSA and incubated overnight at 4C. Slides were then washed three times with PBS and subsequently incubated with 1:200 donkey anti mouse DL 488 (Jackson/Stratech 715-485-150) and 1:200 goat anti-rabbit Cy3 (Jackson/Stratech 111-165-144) in TBS containing DAPI 0.2ug/ml, 10%FBS, 1%BSA for 1 hour at room temperature in the dark. Slides were then washed five times at 10 min each with PBS. Slides were briefly washed in water and air-dried prior to mounting with Mowiol-DABCO and a coverslip. Cells were counted in at least 5 fields for each slide, for a total of over 100 cells per condition.

May-Grunwald-Giemsa staining

$1x10^5$ cells were cytospun for 5min at 300g onto glass slides. Slides were then stained with May-Grunwald solution (Sigma-Aldrich) for 3 min at room temperature. After washing in water, they were incubated for 20min in Giemsa solution (Sigma-Aldrich) (1:20 in water). Slides were washed again in water before being mounted with Mowiol.

Cells were counted in at least 5 fields for each slide, for a total of over 100 cells per condition.

Nitro blue tetrazolium (NBT) reduction assay

NBT reduction assay were performed to determine myeloid differentiation. 0.1% of NBT (final concentration) was added to the liquid culture or semi-solid methocult and incubated at 37^{o}C CO_2 incubator for 3hrs and 12hrs, respectively. Cells were then washed in PBS and the differentiated cells were indicated by the deposition of dark blue insoluble formazan (NBT positive cells) and the percentage of differentiated cells were counted under microscopy. At least 200 cells were counted in most of the cases.

Mouse *Parp1* Knockdown

Scramble or mouse *Parp1* targeting sequences were cloned into pSuper-Retro-Puro retroviral vector (OligoEngine). The target sequences for mouse *Parp-1* gene **(**NM007415.2) are TAAAgAAGCTGACGGTGAA (targeting the position 2014-2032, sh#A)[63], GCCGCCTACTCTATCCTCA (targeting the position 2014-2032, sh#D). The scramble sequence is GCGAAAGATGATAAGCTAA.

Expression of mouse *Parp1* shRNA in NIH3T3 cell line

$1.6x10^5$ cells were plated in each well of 6 well-plates mm and allowed to attach for 6hrs when the cells were infected with 200µl of concentrated virus expressing i) the empty vector, ii) the scramble or iii) shRNA against mouse *Parp1* and 5ug/ml of polybrene in a final volume of 2 ml. After 24 hours, the medium was replaced fresh one containing 1.5µg/ml puromycin (Invitrogen) for a 3-days selection. Cells were then collected for RT-qPCR and Western Blot analysis.

Western blot analysis

Cells were collected by centrifugation and cell pellet was suspended in lysis buffer (0.02% SDS, 0.5% Triton, 300mM NaCl, 20mM Tris-HCl pH 7.5, 1mM EDTA, 1mM DTT, 10mM NaF, 2mM Na_3VO_4) containing 1X protease inhibitors (Roche) and incubated on ice for 30min. Following centrifugation at 16000 g for 15 min at 4°C, the

supernatant containing total cell extract was collected and kept at -80°C. Proteins from cell extracts were quantified using OD660nm Assay (Pierce). 10µg of cell extracts were loaded on a 12% polyacrylamide gel and then electrophoretically transferred onto a Hybond-PVDF membrane (GE Healthcare). The membrane was incubated for 1h at room temperature in blocking buffer (TBS-T containing 8% skimmed milk) to block non-specific protein binding and then incubated at 4°C overnight with the primary antibody, listed in Table S9. Mouse BRCA2 antibody was kindly provided by Dr. Lee. Following four washes with TBS-T, the membrane was incubated for 1 hour with the HPR-conjugated antibody, anti-mouse or anti rabbit (Jackson ImmunoResearch) diluted in blocking buffer. Antibody binding was visualized using the ECL Prime Western blotting detection system (GE Healthcare).

Immunoprecipitation assay

Cells were lysed as above (with a reduced NaCl concentration to 200mM). The 500ug of total cell lysates were incubated with 1ug anti-FLAG antibody at 4°C for 12 hrs with rotation. Then protein-A cojugated beads were added to precipitate the protein complex and incubated at 4°C for 1 hr with rotation. Beads were then washed 5 times with reduced NaCl cell lysis buffer and eluted by 50ul 2% SDS-Tris buffer.

Real time Quantitative PCR

RNA was extracted by using a kit from Fermentas and was reverse transcribed using Super-Script III from Invitrogen. qPCR was performed by using SYBR Green or Taqman probes on an ABI 7900HT Fast Real-Time PCR System (Applied Biosystems) using primers listed in Table S10. *GAPDH* is used a house keeping gene. Relative Expression levels were calculated using the $2^{-\Delta\Delta CT}$ method[64].

***In vivo* plasmid end-joining assay**

In vivo plasmid end-joining assay was performed as described[65]. Briefly a Double Strand Break (DSB) is generated in the *LacZ* gene sequence of the plasmid PUC18 by *Eco*RI digestion. Nuclear extracts from pre-leukemic cells carrying the above mentioned onco-fusion proteins were obtained by using the Nuclear Extraction Kit (Pierce). 2µg of

PUC18 plasmid was digested with *Eco*RI (Fermentas), dephosphorylated (Fermentas), separated on agarose gel 1% and extracted using a column based method (Qiagen). 5ug nuclear extracts were then incubated in NHEJ buffer (50mM Trietanolammine HCL pH7.5, 60mM Potassium Acetate, 0.5mM Magnesium Acetate, 250uM dNTPs, 10mM ATP, 5mM dTT, 500ug/ml BSA) for 5min at 37°C. 250ng of digested-dephosphorylated plasmid were then added to the reaction in 50-100µl final volume and incubated for 24hrs at 18°C. Next day, the DNA was purified using a column based method (Qiagen) and 30ng were used to transform *E. Coli* and plate them on LB-agar plates + 160ug/ml X-Gal (Sigma-Aldrich) and 1mM IPTG (Sigma-Aldrich). Colonies were counted and plotted as shown in Fig. 3i/j. The percentage of misrepair was calculated as the percentage of blue colonies versus total number of colonies.

Homologous Recombination Assay

U2OS cells containing a single copy of the DR-GFP reporter (U2OS-DR) was kindly provided by Dr Maria Jasin. 0.5×10^6 U2OS-DR cells were plated into 6-well plate. After 24 hours, cells were co-transfected with I-SceI expression (pCBASce, 1.25µg), oncogenes of interests (1.25µg) and RFP constructs (0.2µg) using Lipofectamine 2000 (Invitrogen) according to the manufacture's protocol. Percentage of GFP-positive cells was measured by flow cytometry three days after transfection and normalized against percentage of RFP for transfection efficiency. Relative HR efficiency was then normalized to empty vector.

***In vivo* experiments**

All the experimental procedures were approved by King's College London committee and conform to the UK Home office regulations.

We established humanized models of AML1-ETO and PML-RARα leukemia in sub-lethally irradiated NOD/SCID/IL2Rg-/- (NSG, 1 dose 200 RADs) by transplanting $2x10^6$ Kasumi (intra-femoral, IF) and $1x10^5$ NB4-LR2 or $1x10^5$THP1 (intravenous, IV) cells. The day after the transplantation, mice were split into two groups and given intra-peritoneal injections of vehicle (10% HBC) or Olaparib (25mg/kg in 10% HBC) daily for

2-4 weeks. The maximum tolerable dose was calculated by *in vivo* dose-response experiments. Mice were monitored daily until they developed symptoms of leukemia, when they were culled and bone marrow, spleen and liver harvested and analyzed by FACS. The engraftment of human donor cells was defined as human CD45/CD33 double positive by FACS.

For Hoxa9 KO studies, we intravenously injected 10^6 MLL-AF9 leukemic cells (wild type or Hoxa9$^{-/-}$ background) together with $2x10^5$ bone marrow rescue cells into lethally irradiated C57Bl/6 mice (2 doses of irradiation 550RADS each) for disease development. For drug studies, the control cohort received vehicle (10% 2-Hydroxpropyl-beta-cyclodextrin, HBC, Sigma-Aldrich) and the PARPi treatment group received daily Olaparib 50mg/kg in 10% HBC for two-four weeks.

For mouse MLL-AF9 LSC *in vivo* studies involving PARPi and GSK3i, MLL-AF9 LSC were pretreated in R20/20 with 4mM LiCl or 1uM Olaparib or combination for 3 days. Equal number 0.2×10^6 of live cells were transplanted into sublethally irradiated C57Bl6 mice. Continuous Olaparib and LiCO3 treatment was commenced on the day after irradiation and injection of cells. Mice were given 0.4% lithium carbonate containing diet (Harlan Laboratory) along with Olaparib by IP every other day for 4 weeks. The engraftment of mouse donor cells was defined as CD45.1+/ CD45.2- by FACS.

For *in vivo* experiment with primary AML samples, 10^5 AML1 cells transduced with firefly luciferase expressing plasmid were transplanted via by IF into the right femur of the NSG mice. Three days after transplantation, mice were supplemented with 0.4% $LiCO_3$ containing diet and treated with Olaparib as described above for alternative day until day 21. After day 21, mice were maintained on 5 days of lithium carbonate diet and alternated with 2 days regular diet and water for 2 additional weeks. From day 21, the tumor burdens of the animals were detected using IVIS Lumina II® (Caliper) with software Living Image® Verion 4.3.1. Briefly, 100µl of 30mg/mL luciferin were injected into the animals by IP. 10 minutes after injection, the animals were maintained in general anaesthesia by isoflurane and put into the IVIS chamber for photography and

detection of photon emission (large binning, F=1.2, exposure time: 3 mins). The tumor burden were measured and quantified by the same software as instructed. The animals were culled when the tumor burden was 10e8 photon per second or higher.

Microarray and Bioinformatic Analysis

Expression profiles of AML1-ETO (22 samples, cluster13), APL (18 samples, cluster 12), MLL (11 samples, cluster 16) patients were obtained from GEO accession: GSE1159[32]. The data was supported by performing additional gene expression analysis on independent set of published microarray dataset from GSE6891 containing AML1-ETO (37 samples), APL (25 samples), and MLL (35 samples) leukemia samples. All intensity values was adjusted, normalized and summarized in log2 scale using Bioconductor Affy[66] (background correction: rma; normalization: quantiles; summarization: median polish). The differential expression analysis of AML1-ETO and APL against MLL were performed using Bioconductor Limma. The p-values were calculated by paired two-tailed *t*- Test. The selected genes' expression of AML-ETO, APL and MLL were plotted in box-whisker plot using Prism5 software. Gene set enrichment analysis (GSEA) was performed as described[67] using published datasets [44,45].

Statistical Analysis

All the experimental results were analyzed using unpaired two-tailed Student's *t*-Test, 1-way or 2-way ANOVA, as indicated in figure legends. Groups that are statistically compared shared a similar variance as shown in the figures. *p*-values lower than 0.05 were considered statistically significant. The log-rank test was used to compare survival curves.

References

1. Krishnakumar, R. & Kraus, W.L. The PARP side of the nucleus: molecular actions, physiological outcomes, and clinical targets. *Mol Cell* **39**, 8-24 (2010).

2. McLornan, D.P., List, A. & Mufti, G.J. Applying synthetic lethality for the selective targeting of cancer. *N Engl J Med* **371**, 1725-1735 (2014).
3. De Lorenzo, S.B., Patel, A.G., Hurley, R.M. & Kaufmann, S.H. The Elephant and the Blind Men: Making Sense of PARP Inhibitors in Homologous Recombination Deficient Tumor Cells. *Frontiers in oncology* **3**, 228 (2013).
4. Helleday, T. The underlying mechanism for the PARP and BRCA synthetic lethality: clearing up the misunderstandings. *Mol Oncol* **5**, 387-393 (2011).
5. El-Khamisy, S.F., Masutani, M., Suzuki, H. & Caldecott, K.W. A requirement for PARP-1 for the assembly or stability of XRCC1 nuclear foci at sites of oxidative DNA damage. *Nucleic Acids Res* **31**, 5526-5533 (2003).
6. Masson, M.*, et al.* XRCC1 is specifically associated with poly(ADP-ribose) polymerase and negatively regulates its activity following DNA damage. *Mol Cell Biol* **18**, 3563-3571 (1998).
7. Bryant, H.E.*, et al.* PARP is activated at stalled forks to mediate Mre11-dependent replication restart and recombination. *EMBO J* **28**, 2601-2615 (2009).
8. Haince, J.F.*, et al.* PARP1-dependent kinetics of recruitment of MRE11 and NBS1 proteins to multiple DNA damage sites. *J Biol Chem* **283**, 1197-1208 (2008).
9. Haince, J.F.*, et al.* Ataxia telangiectasia mutated (ATM) signaling network is modulated by a novel poly(ADP-ribose)-dependent pathway in the early response to DNA-damaging agents. *J Biol Chem* **282**, 16441-16453 (2007).
10. Paddock, M.N.*, et al.* Competition between PARP-1 and Ku70 control the decision between high-fidelity and mutagenic DNA repair. *DNA repair* **10**, 338-343 (2011).
11. Roy, R., Chun, J. & Powell, S.N. BRCA1 and BRCA2: different roles in a common pathway of genome protection. *Nat Rev Cancer* **12**, 68-78 (2012).
12. Carreira, A.*, et al.* The BRC repeats of BRCA2 modulate the DNA-binding selectivity of RAD51. *Cell* **136**, 1032-1043 (2009).
13. Fong, P.C.*, et al.* Inhibition of poly(ADP-ribose) polymerase in tumors from BRCA mutation carriers. *N Engl J Med* **361**, 123-134 (2009).
14. Tutt, A.*, et al.* Oral poly(ADP-ribose) polymerase inhibitor olaparib in patients with BRCA1 or BRCA2 mutations and advanced breast cancer: a proof-of-concept trial. *Lancet* **376**, 235-244 (2010).
15. Bryant, H.E.*, et al.* Specific killing of BRCA2-deficient tumours with inhibitors of poly(ADP-ribose) polymerase. *Nature* **434**, 913-917 (2005).
16. Farmer, H.*, et al.* Targeting the DNA repair defect in BRCA mutant cells as a therapeutic strategy. *Nature* **434**, 917-921 (2005).
17. Helleday, T., Petermann, E., Lundin, C., Hodgson, B. & Sharma, R.A. DNA repair pathways as targets for cancer therapy. *Nat Rev Cancer* **8**, 193-204 (2008).
18. Esposito, M.T. & So, C.W. DNA damage accumulation and repair defects in acute myeloid leukemia: implications for pathogenesis, disease progression, and chemotherapy resistance. *Chromosoma* (2014).
19. Cheung, N. & So, C.W. Transcriptional and epigenetic networks in haematological malignancy. *FEBS Lett* **585**, 2100-2111 (2011).
20. Zeisig, B.B., Kulasekararaj, A.G., Mufti, G.J. & So, C.W. Acute Myeloid Leukemia: Snapshot. *Cancer Cell* **22**, 698 (2012).

21. Zeisig, B.B. & So, C.W. Retroviral/Lentiviral transduction and transformation assay. *Methods Mol Biol* **538**, 207-229 (2009).
22. Yeung, J.*, et al.* beta-Catenin mediates the establishment and drug resistance of MLL leukemic stem cells. *Cancer Cell* **18**, 606-618 (2010).
23. Smith, L.L.*, et al.* Functional crosstalk between Bmi1 and MLL/Hoxa9 axis in establishment of normal hematopoietic and leukemic stem cells. *Cell Stem Cell* **8**, 649-662 (2011).
24. Arteaga, M.F.*, et al.* The histone demethylase PHF8 governs retinoic acid response in acute promyelocytic leukemia. *Cancer Cell* **23**, 376-389 (2013).
25. Fung, T.K. & So, C.W. Overcoming treatment resistance in acute promyelocytic leukemia and beyond. *Oncotarget* **4**, 1128-1129 (2013).
26. Santos, M.A.*, et al.* DNA-damage-induced differentiation of leukaemic cells as an anti-cancer barrier. *Nature* **514**, 107-111 (2014).
27. Turner, N., Tutt, A. & Ashworth, A. Hallmarks of 'BRCAness' in sporadic cancers. *Nat Rev Cancer* **4**, 814-819 (2004).
28. Kraus, W.L. Transcriptional control by PARP-1: chromatin modulation, enhancer-binding, coregulation, and insulation. *Curr Opin Cell Biol* **20**, 294-302 (2008).
29. Mah, L.J., El-Osta, A. & Karagiannis, T.C. gammaH2AX: a sensitive molecular marker of DNA damage and repair. *Leukemia* **24**, 679-686 (2010).
30. Baumann, P., Benson, F.E. & West, S.C. Human Rad51 protein promotes ATP-dependent homologous pairing and strand transfer reactions in vitro. *Cell* **87**, 757-766 (1996).
31. Moynahan, M.E. & Jasin, M. Mitotic homologous recombination maintains genomic stability and suppresses tumorigenesis. *Nature reviews. Molecular cell biology* **11**, 196-207 (2010).
32. Valk, P.J.*, et al.* Prognostically useful gene-expression profiles in acute myeloid leukemia. *N Engl J Med* **350**, 1617-1628 (2004).
33. Verhaak, R.G.*, et al.* Prediction of molecular subtypes in acute myeloid leukemia based on gene expression profiling. *Haematologica* **94**, 131-134 (2009).
34. Gaymes, T.J., Mufti, G.J. & Rassool, F.V. Myeloid leukemias have increased activity of the nonhomologous end-joining pathway and concomitant DNA misrepair that is dependent on the Ku70/86 heterodimer. *Cancer Res* **62**, 2791-2797 (2002).
35. Pierce, A.J., Johnson, R.D., Thompson, L.H. & Jasin, M. XRCC3 promotes homology-directed repair of DNA damage in mammalian cells. *Genes Dev* **13**, 2633-2638 (1999).
36. Yip, B.H. & So, C.W. Mixed lineage leukemia protein in normal and leukemic stem cells. *Exp Biol Med (Maywood)* **238**, 315-323 (2013).
37. Krivtsov, A.V. & Armstrong, S.A. MLL translocations, histone modifications and leukaemia stem-cell development. *Nat Rev Cancer* **7**, 823-833 (2007).
38. Golub, T.R.*, et al.* Molecular classification of cancer: class discovery and class prediction by gene expression monitoring. *Science* **286**, 531-537 (1999).
39. Costa, B.M.*, et al.* Reversing HOXA9 oncogene activation by PI3K inhibition: epigenetic mechanism and prognostic significance in human glioblastoma. *Cancer Res* **70**, 453-462 (2010).

40. Gaspar, N., *et al.* MGMT-independent temozolomide resistance in pediatric glioblastoma cells associated with a PI3-kinase-mediated HOX/stem cell gene signature. *Cancer Res* **70**, 9243-9252 (2010).
41. Kumar, A.R., *et al.* Hoxa9 influences the phenotype but not the incidence of Mll-AF9 fusion gene leukemia. *Blood* **103**, 1823-1828 (2004).
42. So, C.W., Karsunky, H., Wong, P., Weissman, I.L. & Cleary, M.L. Leukemic transformation of hematopoietic progenitors by MLL-GAS7 in the absence of Hoxa7 or Hoxa9. *Blood* **103**, 3192-3199 (2004).
43. So, C.W., *et al.* MLL-GAS7 transforms multipotent hematopoietic progenitors and induces mixed lineage leukemias in mice. *Cancer Cell* **3**, 161-171 (2003).
44. Faber, J., *et al.* HOXA9 is required for survival in human MLL-rearranged acute leukemias. *Blood* **113**, 2375-2385 (2009).
45. Huang, Y., *et al.* Identification and characterization of Hoxa9 binding sites in hematopoietic cells. *Blood* **119**, 388-398 (2012).
46. Wang, Z., *et al.* GSK-3 promotes conditional association of CREB and its coactivators with MEIS1 to facilitate HOX-mediated transcription and oncogenesis. *Cancer Cell* **17**, 597-608 (2010).
47. Wang, Z., *et al.* Glycogen synthase kinase 3 in MLL leukaemia maintenance and targeted therapy. *Nature* **455**, 1205-1209 (2008).
48. Viale, A., *et al.* Cell-cycle restriction limits DNA damage and maintains self-renewal of leukaemia stem cells. *Nature* **457**, 51-56 (2009).
49. Boichuk, S., Hu, L., Makielski, K., Pandolfi, P.P. & Gjoerup, O.V. Functional connection between Rad51 and PML in homology-directed repair. *PLoS One* **6**, e25814 (2011).
50. Yeung, P.L., *et al.* Promyelocytic leukemia nuclear bodies support a late step in DNA double-strand break repair by homologous recombination. *J Cell Biochem* (2011).
51. Zhong, S., *et al.* A role for PML and the nuclear body in genomic stability. *Oncogene* **18**, 7941-7947 (1999).
52. Alcalay, M., *et al.* Acute myeloid leukemia fusion proteins deregulate genes involved in stem cell maintenance and DNA repair. *J Clin Invest* **112**, 1751-1761 (2003).
53. Armstrong, S.A., *et al.* MLL translocations specify a distinct gene expression profile that distinguishes a unique leukemia. *Nat Genet* **30**, 41-47 (2002).
54. Liu, H., *et al.* Phosphorylation of MLL by ATR is required for execution of mammalian S-phase checkpoint. *Nature* **467**, 343-346 (2010).
55. Rubin, E., *et al.* A role for the HOXB7 homeodomain protein in DNA repair. *Cancer Res* **67**, 1527-1535 (2007).
56. Chiba, N., *et al.* Homeobox B9 induces epithelial-to-mesenchymal transition-associated radioresistance by accelerating DNA damage responses. *Proc Natl Acad Sci U S A* **109**, 2760-2765 (2012).
57. Blanpain, C., Mohrin, M., Sotiropoulou, P.A. & Passegue, E. DNA-damage response in tissue-specific and cancer stem cells. *Cell Stem Cell* **8**, 16-29 (2011).
58. Takacova, S., *et al.* DNA Damage Response and Inflammatory Signaling Limit the MLL-ENL-Induced Leukemogenesis In Vivo. *Cancer Cell* **21**, 517-531 (2012).

59. Santos, M.A., *et al.* DNA-damage-induced differentiation of leukaemic cells as an anti-cancer barrier. *Nature* (2014).
60. Lawrence, H.J., *et al.* Loss of expression of the Hoxa-9 homeobox gene impairs the proliferation and repopulating ability of hematopoietic stem cells. *Blood* **106**, 3988-3994 (2005).
61. Yeung, J. & So, C.W. Identification and characterization of hematopoietic stem and progenitor cell populations in mouse bone marrow by flow cytometry. *Methods Mol Biol* **538**, 301-315 (2009).
62. Dimri, G.P., *et al.* A biomarker that identifies senescent human cells in culture and in aging skin in vivo. *Proc Natl Acad Sci U S A* **92**, 9363-9367 (1995).
63. Choi, E.J., Kim, S.M., Song, K.J., Lee, J.M. & Kee, S.H. Axin1 expression facilitates cell death induced by aurora kinase inhibition through PARP activation. *J Cell Biochem* **112**, 2392-2402 (2011).
64. Schmittgen, T.D. & Livak, K.J. Analyzing real-time PCR data by the comparative C(T) method. *Nat Protoc* **3**, 1101-1108 (2008).
65. Gaymes, T.J., *et al.* Increased error-prone non homologous DNA end-joining--a proposed mechanism of chromosomal instability in Bloom's syndrome. *Oncogene* **21**, 2525-2533 (2002).
66. Gautier, L., Cope, L., Bolstad, B.M. & Irizarry, R.A. affy--analysis of Affymetrix GeneChip data at the probe level. *Bioinformatics* **20**, 307-315 (2004).
67. Martin, N., *et al.* Interplay between Homeobox proteins and Polycomb repressive complexes in p16INK(4)a regulation. *EMBO J* **32**, 982-995 (2013).

Figure Legends

Figure 1: PARPi targets AML1-ETO and PML-RARα leukemic cells *in vitro* and *in vivo*.

a) Relative number of colonies of leukemic cells surviving to PARPi, Olaparib. The number of colonies was acquired after seven days of Olaparib treatment in each round and data was normalized against the vehicle control. Data represents means of six independent experiments ± SD. 1-way ANOVA test was performed between vehicle and Olaparib treated cells for each condition ***$p<0.001$. b) Representative colony morphology with or without Olaparib treatment. Images were acquired using a phase contrast microscope (magnification 40X). c) Relative number of colonies of oncogene-induced leukemic cells transduced either with empty vector or shRNA targeting Parp1. The number of colonies was normalized against empty vector control. Data represents means of at least three independent experiments ± SD. 2-way ANOVA test was performed between empty vector and i) sh-Parp1-A and ii) sh-Parp1-D, *$p<0.05$, **$p<0.01$, ***$p<0.001$. d) Representative colony morphology of leukemic cells transformed by indicated oncoproteins and transduced with empty vector/Parp1 shRNA. Images were acquired using a phase contrast microscopy (magnification 40X). e) Relative number of colonies of human leukemic cell lines Kasumi (AML1-ETO), NB4-LR2 (PML-RARα) and THP1 (MLL-AF9) grown in methylcellulose for 7 days with 5μM Olaparib. The number of colonies after PARPi treatment was normalized against the untreated control. Data represents means of three independent experiments ± SD. 1-way ANOVA test was performed between untreated and Olaparib treated cells for each condition ***$p<0.001$. f) Colony morphology of human leukemic cell lines treated with PARPi (phase contrast microscopy, magnification 40X). Representative pictures are shown. g) Kaplan-Meier survival curve of NSG mice transplanted with Kasumi cell lines (vehicle n=6, Olaparib n=5, pooled from two independent experiments). Log-rank (Mantel-Cox) test was performed between the two curves, $p< 0.01$. h) Kaplan-Meier

survival curve of NSG mice transplanted with NB4-LR2 cell line (vehicle n=5, Olaparib n=10). Log-rank (Mantel-Cox) test was performed between the two curves. $p< 0.05$. i) Kaplan-Meier survival curve of NSG mice transplanted with human THP1cells (vehicle n=5, Olaparib n=5). Log-rank (Mantel-Cox) test was performed between the two curves, p=1.

Figure 2: PARPi induces differentiation, senescence, and apoptosis of AML1-ETO and PML-RARα leukemic cells

a) Giemsa-MacGrunwald staining of leukemic cells showing myeloid differentiation in AML1-ETO and PML-RARα leukemic cells upon treatment with PARPi. b) Quantification of morphologically differentiated cells relating to fig. 2(a). 1-way ANOVA was performed between vehicle and PARPi treated cells ***$p<0.01$. c) Cell cycle analysis of leukemic cells after 48-72hrs of continuous PARPi treatment. Relative percentage of cells in G0-G1, S and G2-M phases are shown. Data represents means of three independent experiments ± SD. 1-way ANOVA was performed between vehicle and PARPi treated cells *$p<0.05$. d-f) Expression of d) *Trp53*, e) *Cdkn1a/p21* and f) *Cdkn2a/p16* in the indicated transformed cells following continuous PARPi treatment. Expression of the target genes was normalized against *Gapdh* ($2^{-\Delta CT}$). Data represents means of three independent experiments ± SD. Unpaired t-test performed between vehicle and PARPi treated cells *$p<0.05$, **$p<0.01$, ***$p<0.001$. g) Detection of primary transformed cells undergoing senescence after 24hrs and 48hrs of PARPi treatment by β-galactosidase staining. Representative pictures are shown (40X magnification). h) Quantification of percentage of β-galactosidase positive cells. Data represents means of three independent experiments ± SD. 1-way ANOVA test was performed between vehicle and PARPi treated cells for each condition at each time point, ***$p<0.001$. i) Quantification of percentage of Annexin V+/PI+ and Annexin V+/PI- cells upon PARPi treatment at 24hrs and 48hrs. Data represents means six independent experiments ± SD. 1-way ANOVA test was performed between untreated and PARPi treated cells for each condition at each time point, ** $p<0.01$.

Figure 3: AML1-ETO and PML-RARα cells show a defect in HR pathway and accumulate DNA damage in response to PARPi treatment.

a) Immunofluorescence microscopy of γH2AX foci in untreated primary transformed mouse cells with the nuclei shown in blue and γH2AX foci in green (representative cells). b) Quantification of the percentage of cells with more than 6 γH2AX foci ± SD in untreated condition. 1-way ANOVA test was performed between 1) AML1-ETO and E2A-PBX, 2) PML-RARα and E2A-PBX, and 3) MLL-AF9 and E2A-PBX (n>3 **p<0.01, *** p<0.001). c) Time-course analysis of PARPi induced γH2AX and RAD51 foci by immunofluorescence upon continuous PARPi treatment with the indicated time. The panels show the nuclei in blue, γH2AX foci in green and RAD51 foci in red (representative cells). d) Quantification of percentage of RAD51 positive cells (> 6 foci) 0hr (white bars), 6hrs (yellow bars) and 24hrs (red bars) upon PARPi treatment is shown. 1-way ANOVA test was performed between untreated and 1) 6hr and 2) (n=4 *p<0.05 ***p<0.001). e) The percentage of cells with γH2AX/RAD51 ratio >2 is shown (n=3 *p<0.05). f) RT-qPCR data of *Rad51, Brca1*, *Brca2*, *Atm, Mcm9 and Rpa1* expression in primary transformed mouse cells. Data represents means of four independent experiments ± SD. 1-way ANOVA was performed between 1) AML1-ETO and MLL-AF9 and 2) PML-RARα and MLL-AF9; *p<0.05, ** p<0.01, *** p<0.001. g) Box-plots showing relative microarray expression of *RAD51*, *ATM, BRCA1, BRCA2, MCM9* and *RPA1* in AML patients carrying the translocation AML1-ETO, PML-RARα (APL) or MLL-fusions. h) Western blot showing the relative expression levels of RAD51, BRAC2 in mouse pre-leukemic cells. Beta ACTIN was used as loading control for quantification to generate the indicated relative signal of the bands. i) Colony forming efficiency as indicative of DSB repair is shown. Repair efficiency is assessed as the total number of bacterial colonies obtained per transformation and expressed as mean ± SEM. 1-way ANOVA was performed between indicated samples (n=3) *p<0.05, *** p<0.001. j) Percentage of misrepair in panel i). Misrepair is calculated as the fraction of white colonies in total (blue and white) colonies, expressed as mean ±SEM. 1-way ANOVA was performed between the indicated samples (n=3) *** p<0.001. k) Efficiency of HR-mediated repair of I-SceI-induced DSB in U2OS/DR-GFP. Cells were transfected with I-SceI, dsRFP and indicated oncogenes or vector control. Data represents relative repair

efficiency calculated as a percentage of repair efficiency measured in cells transfected with empty vector. All data points represents means of three independent experiments±SD. 1-way ANOVA was performed between indicated samples (n=3) *p<0.05, ** p<0.01.

Figure 4: HOXA9 modulates the sensitivity to PARPi

a) Relative colony number of primary transformed cells from wild-type or *Hoxa9*-/- background surviving to PARPi. The number of colonies was counted after seven days culture in methylcellulose with PARPi and normalized against the wild-type control. Data represents means of at least five independent experiments ± SD. 2-way ANOVA test was performed among the data sets: i) wild type vehicle vs *Hoxa9*-/- vehicle, ii) *Hoxa9*-/- vehicle vs *Hoxa9* -/- PARPi **p<0.01, *** p<0.001. b) Representative colony morphology as in Figure 4a (Phase contrast magnification 40X). c) Giemsa-MayGrunwald staining of cells generated with *Hoxa9* -/- mice. d) Detection of senescence by β-galactosidase staining of cells in panel c. e) Quantification of β-galactosidase positive cells in percentage upon 48 hrs PARPi treatment. Data represent means of two independent experiments ± SD. Unpaired two-tailed t-test vehicle and PARPi 48 hrs, *p<0.05 *** p<0.001.f-g) Kaplan-Meier survival curves of C57Bl/6 mice transplanted with MLL-AF9 leukemic cells generated in f) wild type (vehicle n=12, Olaparib n=12 pooled from three independent experiments) and g) *Hoxa9* -/- (vehicle n=14, Olaparib n=11 pooled from three independent experiments) background, respectively. Log-rank (Mantel-Cox) test was performed between the vehicle and the Olaparib group. h) Relative number of colonies of indicated primary transformed cells over-expressing HOXA9 in the presence of PARPi. The number of colonies surviving to 7 days incubation with PARPi was normalized against the vehicle control. Data represents means of three independent experiments ± SD. Two-way ANOVA test was performed among the data sets: 1) wild type vehicle vs wild type PARPi, 2) wild type vehicle vs HOXA9-overexpression PARPi *** p<0.001. i) Colony morphology (phase contrast microscopy, magnification 40X). Representative pictures are shown. j) Giemsa-MayGrunwald staining of primary transformed cells over-expressing HOXA9. k) Detection of senescent cells by β-galactosidase staining. l) Quantification of percentage

of β-galactosidase positive cells upon PARPi treatment for 24 and 48 hrs as in panel k. Data represents means of 2 independent experiments ± SD. 1-way ANOVA test was performed among the data sets: 1) vehicle vs PARPi 24 hrs, 2) vehicle vs PARPi 48hrs, *** $p<0.001$.

Figure 5: HOXA9 modulates PARPi sensitivity

a) Immunofluorescence microscopy of PARPi induced (6 hours) γH2AX and RAD51 foci in wild type and HOXA9 over-expressing cells. Nuclei are shown in blue, γH2AX foci in green and RAD51 are shown in red (representative cells). b) The percentage of 1) γH2AX positive cells (> 6 foci) in wild-type (filled black bars) and HOXA9 over-expressing cells (filled red bars) and 2) RAD51 in wild-type (striped black bars) and HOXA9 over-expressing cells (striped red bars) is shown. Two-way ANOVA test was performed among the data sets: 1) γH2AX in wild-type vs γH2AX in HOXA9 over-expression, 2) RAD51 in wild-type vs RAD51 in HOXA9 over-expression (n=2 **$p<0.01$, ***$p<0.001$). c) Immunofluorescence microscopy of PARPi induced (6 hours) γH2AX and RAD51 foci in MLL-AF9 cells generated in wild type and *Hoxa9-/-* background. Nuclei are shown in blue, γH2AX foci in green and RAD51 are shown in red (representative cells). d) The percentage of 1) γH2AX positive cells (> 6 foci) in wild-type (filled black bars) and *Hoxa9-/-* cells (filled green bars) and 2) RAD51 in wild-type (striped black bars) and *Hoxa9-/-* cells (striped green bars) is shown. Two-way ANOVA test was performed among the data sets 1) γH2AX in wild-type vs γH2AX in *Hoxa9-/-*, 2) RAD51 in wild-type vs RAD51 in *Hoxa9-/-* (n=3 *$p<0.05$). e) Gene Set Enrichment Analysis (GSEA). Genes associated with homologous recombination pathway are enriched in the transcriptional profile of mouse myeloblasts over-expressing Hoxa9. NES, normalized enrichment score; FDR, false discovery rate. f) RTq-PCR showing expression levels of *Rad51* in primary transformed mouse cells over-expressing HOXA9. (Expression levels relative to *Gapdh*, reference control E2A-PBX). Data represents means of four experiments ± SD. Unpaired two-tailed t-test was performed between wild-type vs HOXA9 over-expression *$p<0.05$.) g) RT-qPCR data showing expression levels of *Rad51* in MLL-AF9 cells generated in wild type and *Hoxa9-/-* background. Data represents means of two experiments ± SD. Unpaired two-tailed t-test

was performed between wild-type vs *Hoxa9* KO, *** p<0.001) h) Western blot analysis of Rad51 and Brca2 in MLL-AF9 cells generated in wild-type, *Hoxa9-/- and β-Catenin-/-* background. β-ACTIN was shown as loading control. i) Bar chart shows efficiency of HR-mediated repair of I-SceI-induced DSB in U2OS cells. Cells were transfected with I-SceI, dsRFP and HOXA9 expressing/HOXA9 shRNA plasmids. In the case of HOXA9 over-expression, cells were subjected to 5Gy irradiation 24hrs after transfection. Data is normalised to empty vector or scrambled shRNA. Data represents means of 3 independent experiments ± SD. Unpaired *t-test* was performed between indicated samples (n=3) *p<0.05, ** p<0.01.

Figure 6: Combined PARPi and GSK3i treatment impairs *in vivo* survival of MLL leukemia

a) Relative number of colonies of pre-leukemic cells surviving to PARPi, LiCl or combined PARPi + LiCl treatment. The number of colonies surviving to seven days incubation with drug treatment was normalized against the untreated control. Data represents means of three independent experiments ± SD. 1-way ANOVA was performed among the data sets: 1) vehicle vs PARPi, 2) vehicle vs LiCl, 3) vehicle vs PARPi+ LiCl, 4) PARPi vs PARPi +LiCl, 5) LiCl vs LiCl +PARPi *** p<0.001. b) RT-qPCR data showing expression levels of *c-Myb* in response to PARPi, LiCl or PARPi+LiCl treatment. Data normalized against *Gapdh* levels in untreated MLL-AF9. Data represents means of four independent experiments ± SD. 1-way ANOVA test was performed among the data sets as described in Figure 6a *** p<0.001. c) Relative colony number of leukemic cells surviving to PARPi, LiCl or combined PARPi + LiCl treatment. The number of colonies surviving to seven days incubation with drug treatment was normalized against the vehicle control. Data represents means of four independent experiments ± SD. 1-way ANOVA was performed among the data sets as described in Figure 6a *** p<0.001. d) RT-qPCR data showing expression levels of *c-Myb* in response to PARPi, LiCl or PARPi+LiCl treatment. Data is normalized against *Gapdh* and untreated MLL-AF9. Data represents means of three experiments ± SD. 1-way ANOVA test was performed among the data sets as described in Figure 6b ** p<0.01. e) Giemsa-MayGrunwald staining of leukemic cells over-expressing HOXA9. f) The

percentage of pre-LSC and LSCs undergoing differentiation characterised by morphology (upper panel) and NBT-positive cells (lower panel) following treatment with PARPi, LiCl or in combination for 4 days. 1-way ANOVA was performed among data set as described in Figure 6a. *p<0.05 ***p<0.001. g) Kaplan-Meier survival curves of C57Bl/6 mice transplanted with MLL-AF9 leukemic cells pre-treated in liquid culture with Olaparib, LiCl or Olaparib+LiCl for three days before transplantation (vehicle n=4, Olaparib n=5, LiCl n=5, Olparaib+LiCl n=10). During of *in vivo* treatment is indicted in grey. Log-rank (Mantel-Cox) test was performed between the curves representing the vehicle and the treated groups. p<0.001 for comparison between survival curve representing vehicle and survival curve representing Olaparib+LiCl treatment. h-i) Relative proliferation of primary human MLL samples from h) AML1 (t11;17) and i) AML-2 (t6;11) with LiCl (8mM), PARPi (1uM Olaparib) or the combined PARPi+LiCl treatment. Cells were counted by trypan blue exclusion 5 days after PARPi treatment. The data show the fold change in cell number relative to day 0. Data represents means of at least two independent experiments ± SD. 1-way ANOVA test was performed among the data sets as described in Figure 6a *p<0.05; ** p<0.01; *** p<0.001. j) Giemsa-MayGrunwald staining of human leukemic cells upon indicated treatments. k) The percentage of primary leukemic cells undergoing differentiation characterised by morphology (left panel) and NBT positive cells (right panel) following treatment with PARPi, LiCl or combination for 5 days. 1-way ANOVA was performed among the data sets as described in Figure 6a. **p<0.01 ***p<0.001. l) Results of *in vivo* imaging of disease progression of mice transplanted with AML1 primary human leukemic cells carrying luciferase reporter upon treatments. Left panel: Quantification of tumour burden measured as photon per second*10E+03 in NSG mouse 28 days after transplantation with primary human MLL cells. Right: Fold change in tumor burden between Day 28 and Day 21 after the transplant. Low level of tumor burden was detectable at Day 21. 1-way ANOVA was performed between vehicle and treated group. ** p<0.001. m) Kaplan-Meier survival curves of NSG mice transplanted with AML1 leukemic cells (vehicle n=6, Olaparib n=6, LiCl n=6, Olparaib +LiCl n=6). Duration of *in vivo* treatment is indicted in grey. Log-rank (Mantel-Cox) test was performed between the curves representing the

vehicle and the treated groups. **p<0.01 for comparison between survival curve representing vehicle and the survival curve representing Olaparib+LiCl treatment.

Supplementary Figure 1 (data related to Figure 1): PARPi targets AML1-ETO and PML-RARα leukemic cells *in vitro* and *in vivo*.

a) Non-linear regression dose response curve of Olaparib treatment in normal mouse bone marrow c-Kit$^+$ cells grown in methylcellulose for 7 days. Data represents means of three independent experiments ± SD. The EC50, the half maximal effective concentration, of Olaparib for the cells is indicated. b) Colony morphology of c-Kit$^+$ normal mouse bone marrow cells (Phase contrast microscopy magnification 40X). Representative pictures are shown. c) Absolute colonies number of leukemic cells surviving to Olaparib treatment corresponding to Fig. 1a. Data represents means of six independent experiments ± SEM. d) Non-linear regression dose response curve of leukemic cells as indicated grown in methylcellulose for 7 days with escalating doses of PARPi. Data represents mean of three independent experiments are shown. The EC50 of Olaparib for the cells is indicated. e) Relative colonies number of leukemic cells surviving to PARPi, Veliparib. The number of colonies surviving to seven days incubation with Veliparib treatment was normalized against the untreated control. Data represents means of three independent experiments ± SD. unpaired two-tailed t-test was performed between vehicle and Veliparib treated cells for each condition ***p<0.001. f) Representative morphology of colonies indicated in Supplementary Fig. 1e (phase contrast microscopy, magnification 20X). g) Efficiency of *Parp1* Knockdown (KD) in NIH3T3 cells transduced with retroviral vectors expressing shRNA targeting against mouse *Parp1*. RT-qPCR data showing expression of *Parp1* in NIH3T3 transduced with sh-mParp1. Data represents means of two independent experiments ± SD. 1-way ANOVA test was performed between empty vector and 1) sh-Parp1-A and 2) sh-Parp1-D ***p<0.001. h) RT-qPCR showing *Parp1* KD efficiency in primary cells transformed by the indicated fusion proteins. Data represents means of three independent experiments ±

SD. 1-way ANOVA test was performed between empty vector and 1) sh-Parp1-A and 2) sh-Parp1-D *p<0.05, **p<0.01, ***p<0.001. i**)** Absolute colonies numbers from the indicated primary transformed cells after shRNA-mediated *Parp1* KD, corresponding to Fig. 1c. Data represents means of more than three independent experiments ± SD. j-l) Flow cytometry analysis of bone marrow, spleen and liver harvested from sick mice transplanted with j) Kasumi, k) NB4-LR2 cell and l) THP1 respectively confirming level of engraftment. m-o) Giemsa-MayGrunwald staining of cells harvested from bone marrow, spleen or tumor of sick mice succumbed transplanted with m) Kasumi, n) NB4-LR2 and o) THP1 respectively. Bright field microscopy (40x). Representative pictures are shown. p) Non-linear regression dose response curve of primary AML patient cells to Olaparib. Primary patients cells were treated with PARPi for 5 days. Data represents means of three independent experiments ± SD. q) EC50 of MLL, APL and AML-ETO primary patient samples to Olaparib. 1-way ANOVA was performed between 1) MLL and APL patients samples 2) MLL and AML1-ETO patients samples. ** p<001.

Supplementary Figure 2 (data related to Figure 2): PARPi induces differentiation, senescence, and apoptosis of AML1-ETO and PML-RARα leukemic cells

a) Proliferation of pre-leukemic cells in the presence and absence of PARPi in methylcellulose at indicated time point. b) Giemsa-MacGrunwald staining of primary transformed cells with PARPi treatment at indicated time points. Representative pictures are shown. c) Percentage of differentiated cells counted according to morphology from figures shown in panel (b). Unpaired two-tailed t-test was performed between cells treated with vehicle or PARPi for 2, 4 and 6 days. *p<0.01, ***p<0.001. d) Percentage of NBT positive cells. Data represents means of three independent experiments ± SD. Unpaired two-tailed t-test was performed between cells treated with vehicle or PARPi for 2, 4 and 6 days. *** p<0.001. e) Representative cell cycle profiles related to Fig. 2c. f) Representative FACS profile (Annexin V/PI) of pre-leukemic cells treated with PARPi related to Fig. 2i. g) Detection of senescent cells by β-galactosidase staining in human leukemic cell lines after 72hrs of PARPi treatment. h) Quantification of percentage of β-galactosidase positive in human leukemic cells following PARPi treatment. Data represents means of two independent experiments ± SD. Unpaired t-test was performed

between vehicle and PARPi treated cells, ***p<0.001. i) Quantification of apoptotic cells in human leukemic cell lines in percentage upon 4 days PARPi treatment. Data represents means of four independent experiments, ± SD. Unpaired two-tailed t-test was performed between vehicle and PARPi *** p<0.001. j) Giemsa-Mayrunwald staining of human primary AML cells upon 1μM Olaparib treatment for 5 days. The red arrow indicates the differentiated cells. k) Quantification of morphologically differentiated cells relating to panel 2j. Data represents means of two independent experiments ± SD. Unpaired t-test was performed between cells treated with vehicle and PARPi **p<0.01. l) Percentage of NBT positive cells after PARPi treatment for 5 days. Data represents mean of three independent experiments ± SD. Unpaired t-test test was performed between cells treated with vehicle and PARPi *p<0.05, *** p<0.001.

Supplementary Figure 3 (data related to Figure 3): AML1-ETO and PML-RARα cells show a defect in HR pathway and accumulate DNA damage in response to PARPi treatment.

a) Western blot showing endogenous PARP1 co-immunoprecipitates with APLF (positive control) but not the oncofusion proteins in transfected 293T cells. b-e) RT-qPCR showing the effect of *Parp1* KD on b) AML-1-ETO, c) PML-RARα, d) MLL-AF9 and e) E2A-PBX target genes. Data represents means of two independent experiments ± SD. 1-way ANOVA test was performed between 1) Scrambled and shParp1-A; 2) Scrambled and shParp1-D. *p<0.05, **p<0.01. f) The percentage of cells with >10 γH2AX foci± SEM in untreated condition is shown, and exhibits similar results by counting >6 γH2AX foci in Fig. 3b. 1-way ANOVA was performed between: 1) AML1-ETO and E2A-PBX, 2) PML-RARα and E2A-PBX, 3) MLL-AF9 and E2A-PBX, 4) AML1-ETO and MLL-AF9, 5) PML-RARα and MLL-AF9 (n=7, *p<0.05, ** p<0.01, ***p<0.001). g-j) Time-course analysis of PARPi induced γH2AX and RAD51 foci by immunofluorescence microscopy in g) AML1-ETO, h) PML-RARα, i) MLL-AF9 and j) E2A-PBX cells . The panels show the nuclei in blue, γH2AX foci in green and RAD51 foci in red. k). The percentage of γH2AX positive cells (> 6 foci) 0 (white bars), 6 (yellow bars) and 24 hrs (red bars) upon PARPi treatment is shown. 1-way ANOVA was performed between untreated and 1) 6hr and 2) 24hr (n=4 *p<0.05, ***p<0.001). l) The

figure shows the percentage of RAD51 positive cells (>10 foci), 0 (white bars), 6 (yellow bars) and 24hrs (red bars) upon PARPi treatment. 1-way ANOVA test was performed between: 1) untreated and 6hrs and 2) untreated and 24hrs post treatment (n=4, ***p<0.001). Consistent results were obtained by counting >6 Rad51 foci in Fig. 3d. m) Cell cycle analysis of indicated primary transformed cells treated with vehicle or PARPi for 6hrs (left) and 24hrs (right). n) Immunofluorescence microscopy for γH2AX foci in untreated human cells with nuclei in blue (DAPI) and γH2AX foci in green (representative cells). o) The percentage of cells with >6 γH2AX foci ± SD in untreated condition. 1-way ANOVA was performed between: 1) Kasumi and THP1 and 2) NB4 and THP1 ** p<0.01 p) Time-course analysis of PARPi induced γH2AX and RAD51 foci by immunofluorescence microscopy in human leukemic cell lines. The panels show the nuclei in blue, γH2AX foci in green and RAD51 foci in red (representative cells). q) The percentage of RAD51 positive human cells (> 6 foci) 0 (white bars), 6 hrs (yellow bars) and 24 hrs (red bars) upon PARPi treatment. 1-way ANOVA test was performed between untreated and 6hr (n=4 **p<0.01). r) The percentage of cells with γH2AX/RAD51 ratio >2, Unpaired t-test was performed with ** p<0.01. s) Box-plot showing normalized expression of DNA repair-associated genes in AML patient samples from Verhaak et al., Haematologica 2009. AML1-ETO n=37, APL n=25, MLL n=35). *p<0.05, **p<0.01, ***p<0.001, NS=Not Significant, p values were calculated using unpaired *t*-Test.

Supplementary Figure 4 (data related to Figure 4): HOXA9 modulates the sensitivity to PARPi

a) RT-qPCR data showing expression of human *HOXA9* in U937 cell lines carrying Zinc (Zn)-inducible *AML1-ETO* or *PML-RARα* 6hrs after the induction. . Data represents means of two independent experiments ± SD. 2-way ANOVA test was performed between untreated and Zinc induced cells (**p<0.01). b) RT-qPCR data showing expression of mouse *Hoxa9* in primary transformed cell line expressing inducible MLL-AF9-ER after tamoxifen withdrawal at indicated time points. Data represents means of three independent experiments ± SD. 1-way ANOVA test was performed between Day 0 (untreated) and Day 3, Day 0 and Day 5 (*p<0.05, *p<0,001). c) Normalized expression

of *HOXA9* in AML patient samples from Verhaak et al., Haematologica 2009 (Left) and Valk et al., NEJM 2004 (Right), ***p<0.001, NS=Not Significant, p-values were calculated using unpaired t-test. d) Semi-quantitative PCR showing the genotype of cells generated in wild type and *Hoxa9*-/- background. e) Absolute colony number of primary transformed cells generated in wild-type or *Hoxa9*-/- background surviving to PARPi. Data represent means of five independent experiments ± SEM, corresponding to data in Fig. 4a. f) Flow cytometry analysis (c-Kit/Gr1 and c-Kit/Mac1) of primary transformed cells before and after PARPi treatment. g) Kaplan-Meier survival curves of C57Bl/6 mice serially transplanted with MLL-AF9 cells generated in *Hoxa9* $^{-/-}$ (bold black line, n=5) and wild type (bold red line, n=3) background. The leukemic cells harvested from mice succumbed with leukemia (primary recipients) were transplanted in C57Bl/6 recipient mice (secondary transplants, dotted lines, n=9 and n=3). h) Flow cytometry analysis (CD45.1/CD45.2, Gr1/c-Kit, Gr1/Mac1) of bone marrow harvested from mice treated as indicated. wild type (left) and *Hoxa9* $^{-/-}$ (right). Engrafted cells were labelled by CD45.1. i) Absolute colony number of primary transformed cells over-expressing HOXA9 surviving to PARPi, corresponding to data shown in Figure 4h. Data represent means of three independent experiments ± SEM. j) RT-qPCR data showing expression of *Hoxa9* and their respective oncogenes in transformed mouse cells before and after Hoxa9 over-expression. Data represents means of two independent experiments ± SD. Unpaired two tailed t-test was performed between wild type vs Hoxa9 over-expression n=4, *p<0.05, ** p<0.01, *** p<0.001.

Supplementary Figure 5 (related to Figure 5): HOXA9 modulates PARPi sensitivity

a-b) Gene Sets Enrichment Analysis (GSEA). Gene sets associated with DNA repair (a) and double strand break repair (b) are enriched in the transcriptional profile of mouse myeloblasts over-expressing HOXA9. c) RT-qPCR of DDR genes in MLL-AF9 wild type and MLL-AF9 Hoxa9 KO cells. Gene expressions in MLL-AF9 wild-type were normalized to 1. Data represents means of two independent experiments ± SD. 1-way ANOVA test was performed between untreated and PARPi treated cells (***$p<0.001$).

Supplementary Figure 6 (data related to Figure 6): Combined PARPi and GSK3i treatment impairs *in vivo* survival of MLL leukemia

a) Non-linear regression dose response curve of GSK3i (LiCl) in c-Kit+ normal mouse bone marrow cells grown in methylcellulose. Colony number was acquired after 7 days of culture. Data represents means of three independent experiments±SD. EC50 (50% of maximal effective concentration) are indicated in the figure. b-c) Absolute colony number of b) pre-LSC c) LSC surviving to PARPi, LiCl or combined PARPi+LiCl treatment. Relative number of colony is shown in Figure 6a and c. Data represents means of three independent experiments ± SEM. 1-way ANOVA test. **$p<0.01$, ***$p<0.001$. Data represents means of four independent experiments±SEM. 1-way ANOVA test ***$p<0.001$. d) Flow cytometry analysis (CD45.1/CD45.2, c-kit/Gr1, Gr1/Mac1) of bone marrow harvested from C57Bl6 mice transplanted with CD45.1 positive MLL-AF9 cells. e) Giemsa-MayGrunwald staining of cells harvested from bone marrow of sick animals with indicated treatments. f) Relative proliferation of human leukemic cells THP1 to LiCl, PARPi or combined PARPi+LiCl treatment. Cells were counted on day 5 after treatment by trypan blue exclusion. The data show the fold change in cell number relative to day 0. Data represents means of at least two independent experiments ± SD. 1-way ANOVA Test was performed among the data sets: 1) untreated vs PARPi, 2) untreated vs LiCl, 3) untreated vehicle vs PARPi+ LiCl, 4) PARPi vs PARPi +LiCl, 5) LiCl vs LiCl +PARPi ** $p<0.01$; *** $p<0.001$. g) Giemsa-MayGrunwald staining of human THP1 cells with indicated treatments. h) Pictures showing the tumor burden of each treatment group that are visualized and quantified in Figure 6l. i) Flow cytometry analysis (CD45/CD33) of bone marrow harvested from sick NSG mice transplanted with

primary AML1 cells undergone indicated treatments. j) Giemsa-MayGrunwald staining of cells harvested from bone marrow of sick mice with indicated treatment.

Supplementary Figure 7: Proposed models for PARPi treatments in different AML subtypes driven by oncogenic transcription factors.

AML1-ETO and PML-RARα suppress the expression of DDR gene and HR efficiency, which make them sensitive to PARPi treatment. In contrast, leukemia driven by MLL-fusion expressing a high level of HR genes including *HOXA9* is refractory to PARPi. Inactivation of *HOXA9* by genetic mean or GSK3i can re-sensitize MLL leukemia to PARPi, and suppresses disease development.

Figure 1

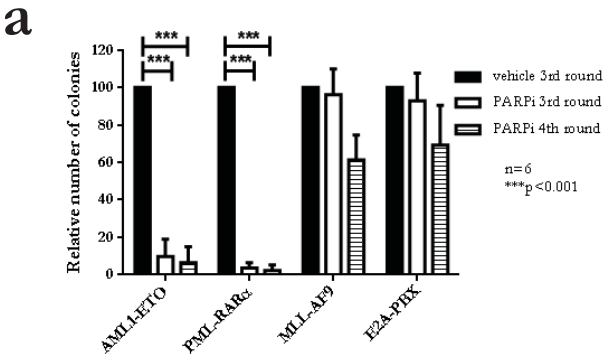
a
Relative number of colonies
vehicle 3rd round
PARPi 3rd round
PARPi 4th round
n=6
***p<0.001
AML1-ETO
PML-RARα
MLL-AF9
E2A-PBX

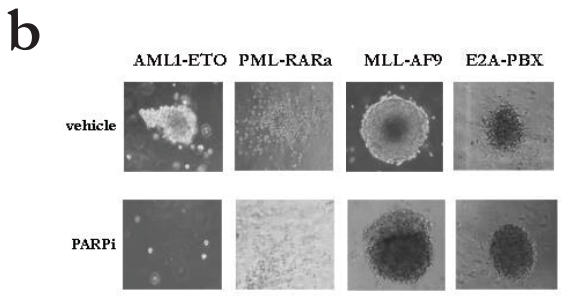
b
AML1-ETO
PML-RARa
MLL-AF9
E2A-PBX
vehicle
PARPi

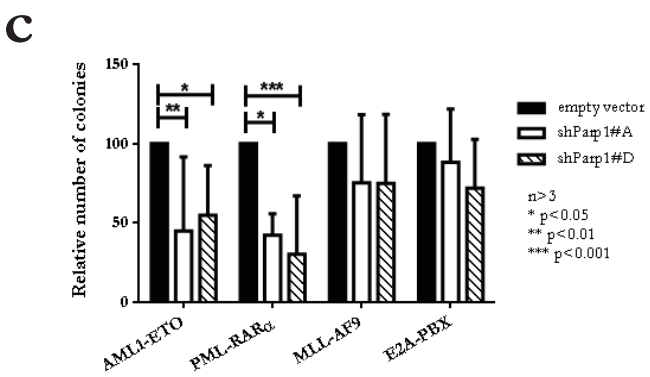
c
Relative number of colonies
empty vector
shParp1#A
shParp1#D
n>3
* p<0.05
** p<0.01
*** p<0.001
AML1-ETO
PML-RARα
MLL-AF9
E2A-PBX

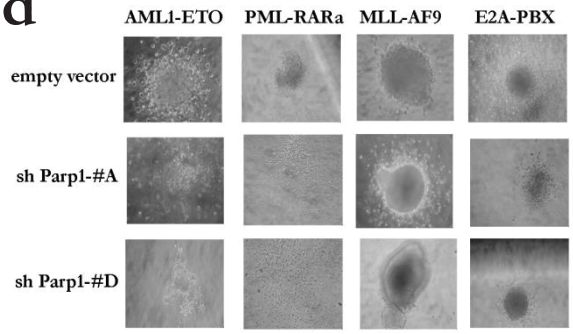
d
AML1-ETO
PML-RARa
MLL-AF9
E2A-PBX
empty vector
sh Parp1-#A
sh Parp1-#D

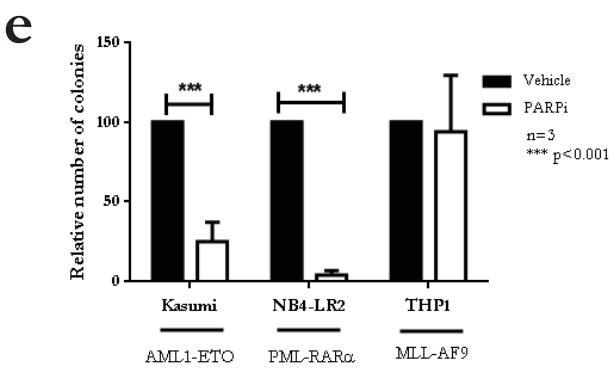
e
Relative number of colonies
Vehicle
PARPi
n=3
*** p<0.001
Kasumi
NB4-LR2
THP1
AML1-ETO
PML-RARα
MLL-AF9

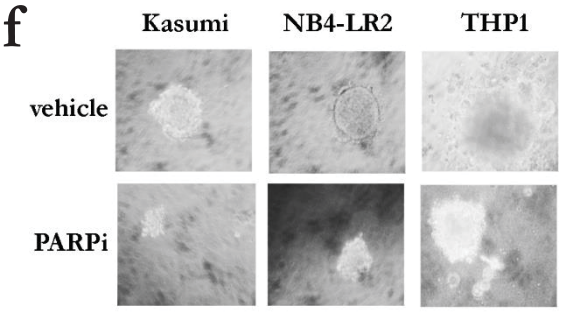
f
Kasumi
NB4-LR2
THP1
vehicle
PARPi

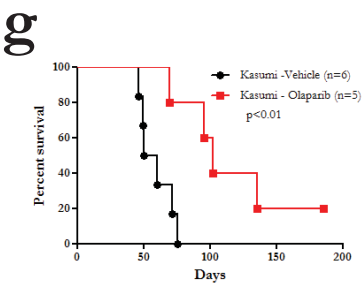
g
Kasumi -Vehicle (n=6)
Kasumi - Olaparib (n=5)
p<0.01
Percent survival
Days

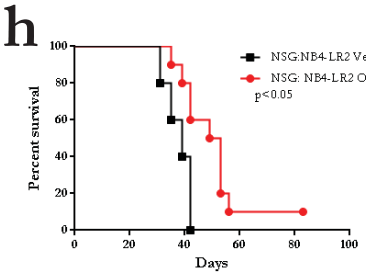
h
NSG:NB4-LR2 Vehicle (n=5)
NSG: NB4-LR2 Olaparib (n=10)
p<0.05
Percent survival
Days

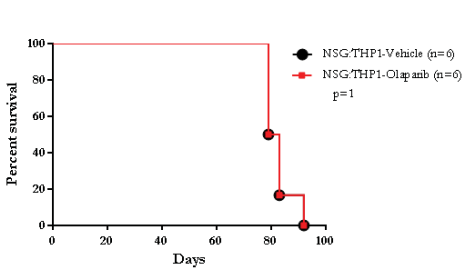
i
NSG/THP1-Vehicle (n=6)
NSG/THP1-Olaparib (n=6)
p=1
Percent survival
Days

Figure 2

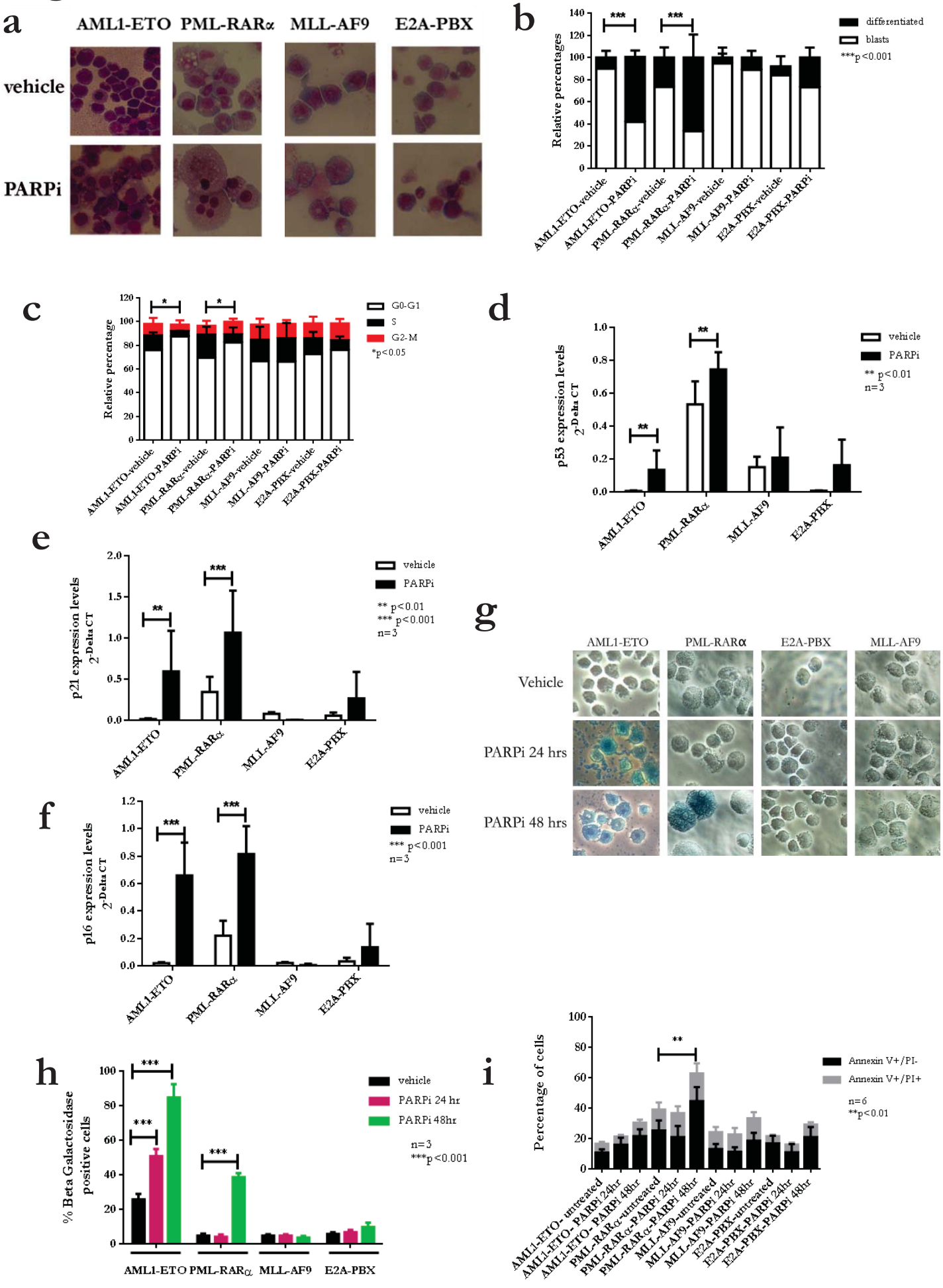
a
AML1-ETO
PML-RARα
MLL-AF9
E2A-PBX
vehicle
PARPi
b
differentiated
blasts
***p<0.001
Relative percentages
AML1-ETO-vehicle
AML1-ETO-PARPi
PML-RARα-vehicle
PML-RARα-PARPi
MLL-AF9-vehicle
MLL-AF9-PARPi
E2A-PBX-vehicle
E2A-PBX-PARPi
c
G0-G1
S
G2-M
*p<0.05
Relative percentage
d
vehicle
PARPi
** p<0.01
n=3
p53 expression levels
2-Delta CT
AML1-ETO
PML-RARα
MLL-AF9
E2A-PBX
e
vehicle
PARPi
** p<0.01
*** p<0.001
n=3
p21 expression levels
2-Delta CT
f
vehicle
PARPi
*** p<0.001
n=3
p16 expression levels
2-Delta CT
g
AML1-ETO
PML-RARα
E2A-PBX
MLL-AF9
Vehicle
PARPi 24 hrs
PARPi 48 hrs
h
vehicle
PARPi 24 hr
PARPi 48hr
n=3
***p<0.001
% Beta Galactosidase positive cells
AML1-ETO
PML-RARα
MLL-AF9
E2A-PBX
i
Annexin V+/PI-
Annexin V+/PI+
n=6
**p<0.01
Percentage of cells
AML1-ETO- untreated
AML1-ETO- PARPi 24hr
AML1-ETO- PARPi 48hr
PML-RARα-untreated
PML-RARα-PARPi 24hr
PML-RARα-PARPi 48hr
MLL-AF9-untreated
MLL-AF9-PARPi 24hr
MLL-AF9-PARPi 48hr
E2A-PBX-untreated
E2A-PBX-PARPi 24hr
E2A-PBX-PARPi 48hr

Figure 3

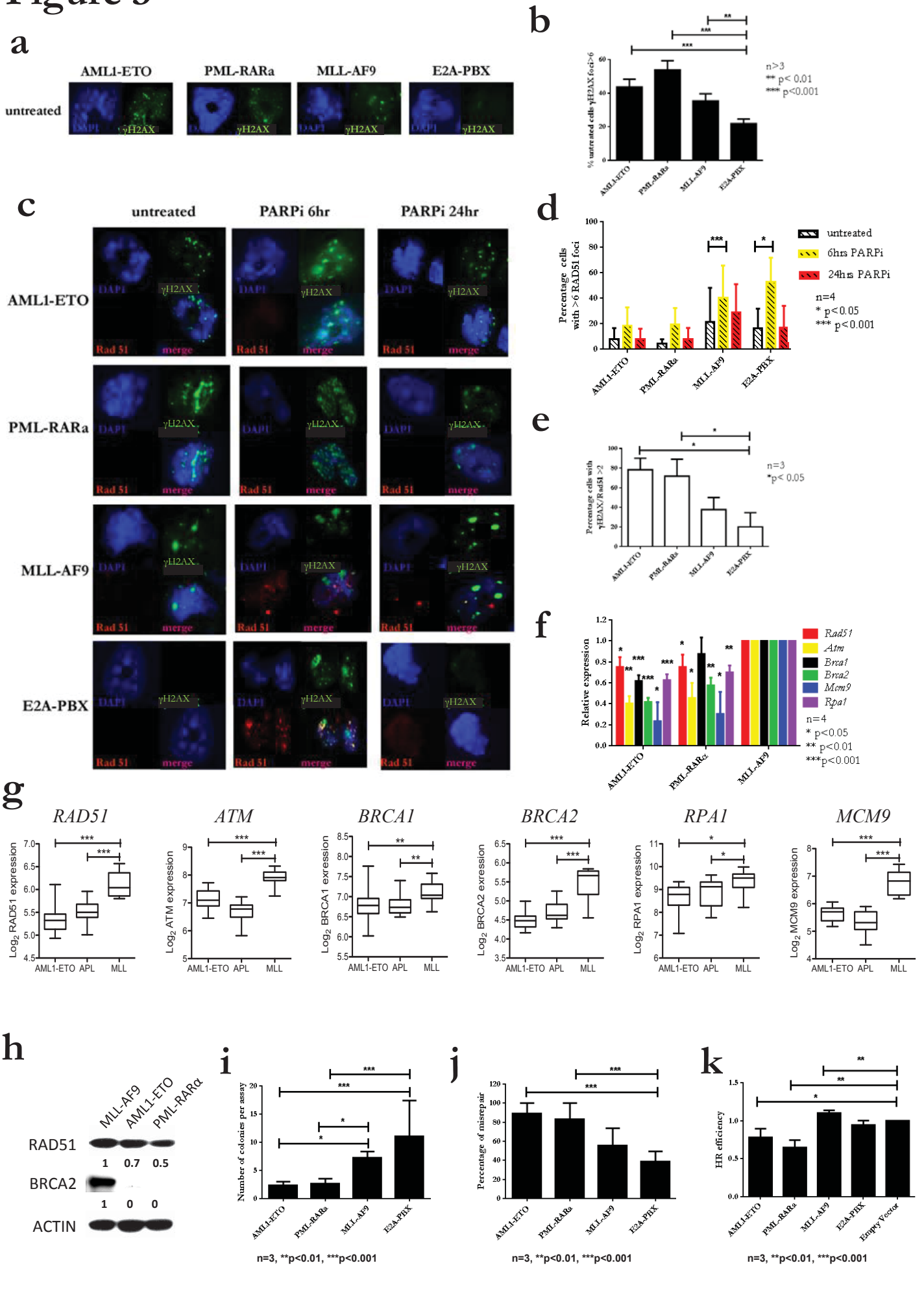
a
AML1-ETO
PML-RARa
MLL-AF9
E2A-PBX
untreated
DAPI
γH2AX
b
% untreated cells γH2AX foci>6
n>3
** p< 0.01
*** p<0.001
c
untreated
PARPi 6hr
PARPi 24hr
AML1-ETO
PML-RARa
MLL-AF9
E2A-PBX
Rad 51
merge
d
Percentage cells with >6 RAD51 foci
untreated
6hrs PARPi
24hrs PARPi
n=4
* p<0.05
*** p<0.001
e
Percentage cells with γH2AX/Rad51 >2
n=3
*p< 0.05
f
Relative expression
Rad51
Atm
Brca1
Brca2
Mcm9
Rpa1
n=4
* p<0.05
** p<0.01
***p<0.001
PML-RARα
g
RAD51
ATM
BRCA1
BRCA2
RPA1
MCM9
Log2 RAD51 expression
Log2 ATM expression
Log2 BRCA1 exression
Log2 BRCA2 exression
Log2 RPA1 expression
Log2 MCM9 expression
AML1-ETO APL MLL
h
MLL-AF9
AML1-ETO
PML-RARα
RAD51
1 0.7 0.5
BRCA2
1 0 0
ACTIN
i
Number of colonies per assay
n=3, **p<0.01, ***p<0.001
j
Percentage of misrepair
n=3, **p<0.01, ***p<0.001
k
HR efficiency
Empty Vector
n=3, **p<0.01, ***p<0.001

Figure 4

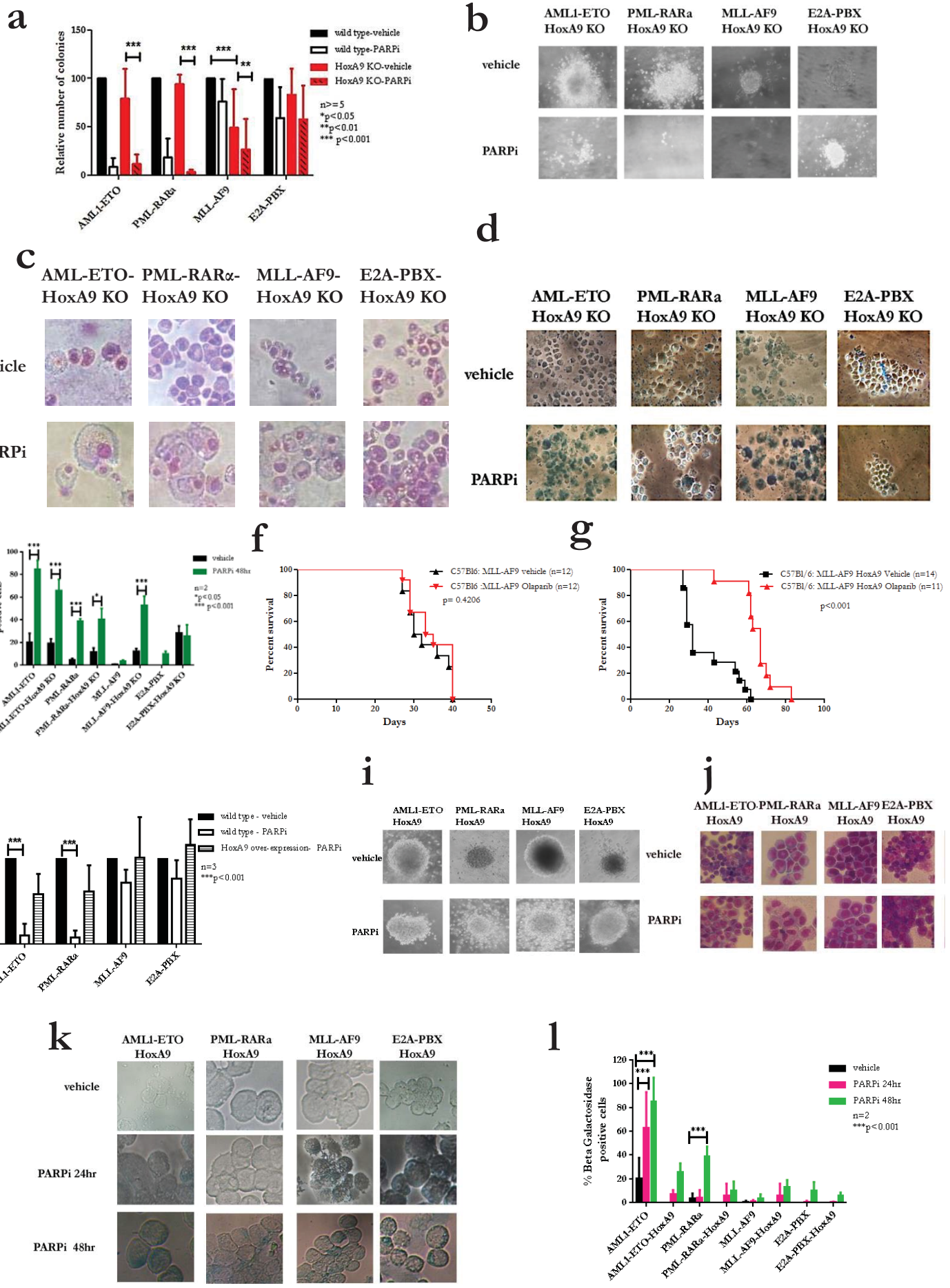
a
Relative number of colonies
wild type-vehicle
wild type-PARPi
HoxA9 KO-vehicle
HoxA9 KO-PARPi
n>=5
*p<0.05
**p<0.01
*** p<0.001
AML1-ETO
PML-RARa
MLL-AF9
E2A-PBX
b
AML1-ETO HoxA9 KO
PML-RARa HoxA9 KO
MLL-AF9 HoxA9 KO
E2A-PBX HoxA9 KO
vehicle
PARPi
c
AML-ETO-HoxA9 KO
PML-RARα-HoxA9 KO
MLL-AF9-HoxA9 KO
E2A-PBX-HoxA9 KO
Vehicle
PARPi
d
AML-ETO HoxA9 KO
PML-RARa HoxA9 KO
MLL-AF9 HoxA9 KO
E2A-PBX HoxA9 KO
vehicle
PARPi
e
% Beta Galactosidase positive cells
vehicle
PARPi 48hr
n=2
*p<0.05
*** p<0.001
AML1-ETO
AML1-ETO-HoxA9 KO
PML-RARa
PML-RARa-HoxA9 KO
MLL-AF9
MLL-AF9-HoxA9 KO
E2A-PBX
E2A-PBX-HoxA9 KO
f
Percent survival
C57Bl6: MLL-AF9 vehicle (n=12)
C57Bl6 :MLL-AF9 Olaparib (n=12)
p= 0.4206
Days
g
Percent survival
C57Bl/6: MLL-AF9 HoxA9 Vehicle (n=14)
C57Bl/6: MLL-AF9 HoxA9 Olaparib (n=11)
p<0.001
Days
h
Relative number of colonies
wild type - vehicle
wild type - PARPi
HoxA9 over-expression- PARPi
n=3
***p<0.001
AML1-ETO
PML-RARa
MLL-AF9
E2A-PBX
i
AML1-ETO HoxA9
PML-RARa HoxA9
MLL-AF9 HoxA9
E2A-PBX HoxA9
vehicle
PARPi
j
AML1-ETO HoxA9
PML-RARa HoxA9
MLL-AF9 HoxA9
E2A-PBX HoxA9
vehicle
PARPi
k
AML1-ETO HoxA9
PML-RARa HoxA9
MLL-AF9 HoxA9
E2A-PBX HoxA9
vehicle
PARPi 24hr
PARPi 48hr
l
% Beta Galactosidase positive cells
vehicle
PARPi 24hr
PARPi 48hr
n=2
***p<0.001
AML1-ETO
AML1-ETO-HoxA9
PML-RARa
PML-RARa-HoxA9
MLL-AF9
MLL-AF9-HoxA9
E2A-PBX
E2A-PBX-HoxA9

Figure 5

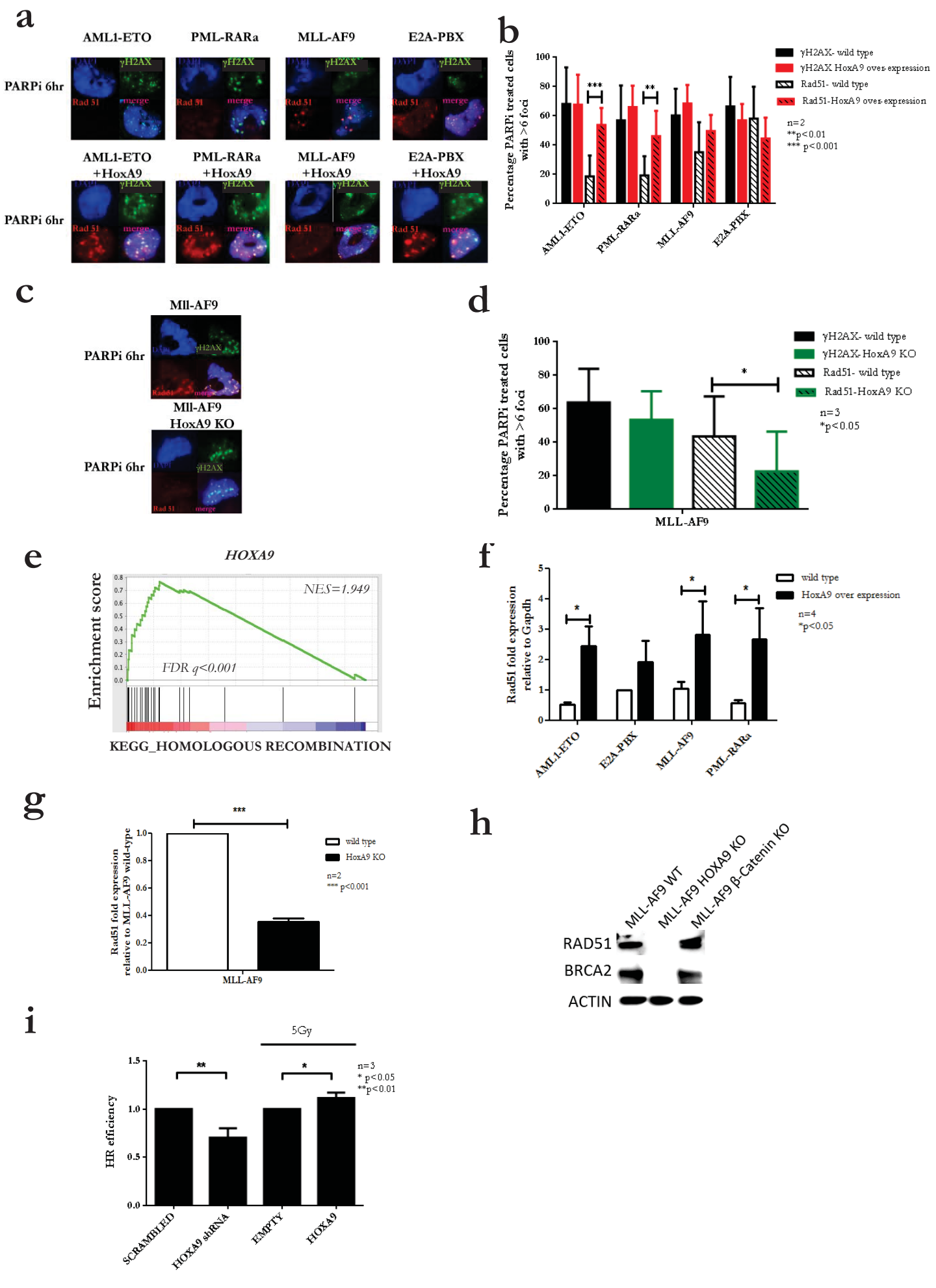
a
AML1-ETO
PML-RARa
MLL-AF9
E2A-PBX
PARPi 6hr
AML1-ETO +HoxA9
PML-RARa +HoxA9
MLL-AF9 +HoxA9
E2A-PBX +HoxA9
PARPi 6hr
γH2AX
Rad 51
merge
b
Percentage PARPi treated cells with >6 foci
γH2AX- wild type
γH2AX HoxA9 over-expression
Rad51- wild type
Rad51-HoxA9 over-expression
n=2
**p<0.01
*** p<0.001
AML1-ETO
PML-RARa
MLL-AF9
E2A-PBX
c
Mll-AF9
PARPi 6hr
Mll-AF9 HoxA9 KO
PARPi 6hr
d
Percentage PARPi treated cells with >6 foci
γH2AX- wild type
γH2AX-HoxA9 KO
Rad51- wild type
Rad51-HoxA9 KO
n=3
*p<0.05
MLL-AF9
e
HOXA9
Enrichment score
NES=1.949
FDR q<0.001
KEGG_HOMOLOGOUS RECOMBINATION
f
Rad51 fold expression relative to Gapdh
wild type
HoxA9 over expression
n=4
*p<0.05
AML1-ETO
E2A-PBX
MLL-AF9
PML-RARa
g
Rad51 fold expression relative to MLL-AF9 wild-type
wild type
HoxA9 KO
n=2
*** p<0.001
MLL-AF9
h
MLL-AF9 WT
MLL-AF9 HOXA9 KO
MLL-AF9 β-Catenin KO
RAD51
BRCA2
ACTIN
i
5Gy
HR efficiency
n=3
* p<0.05
**p<0.01
SCRAMBLED
HOXA9 shRNA
EMPTY
HOXA9

Figure 6

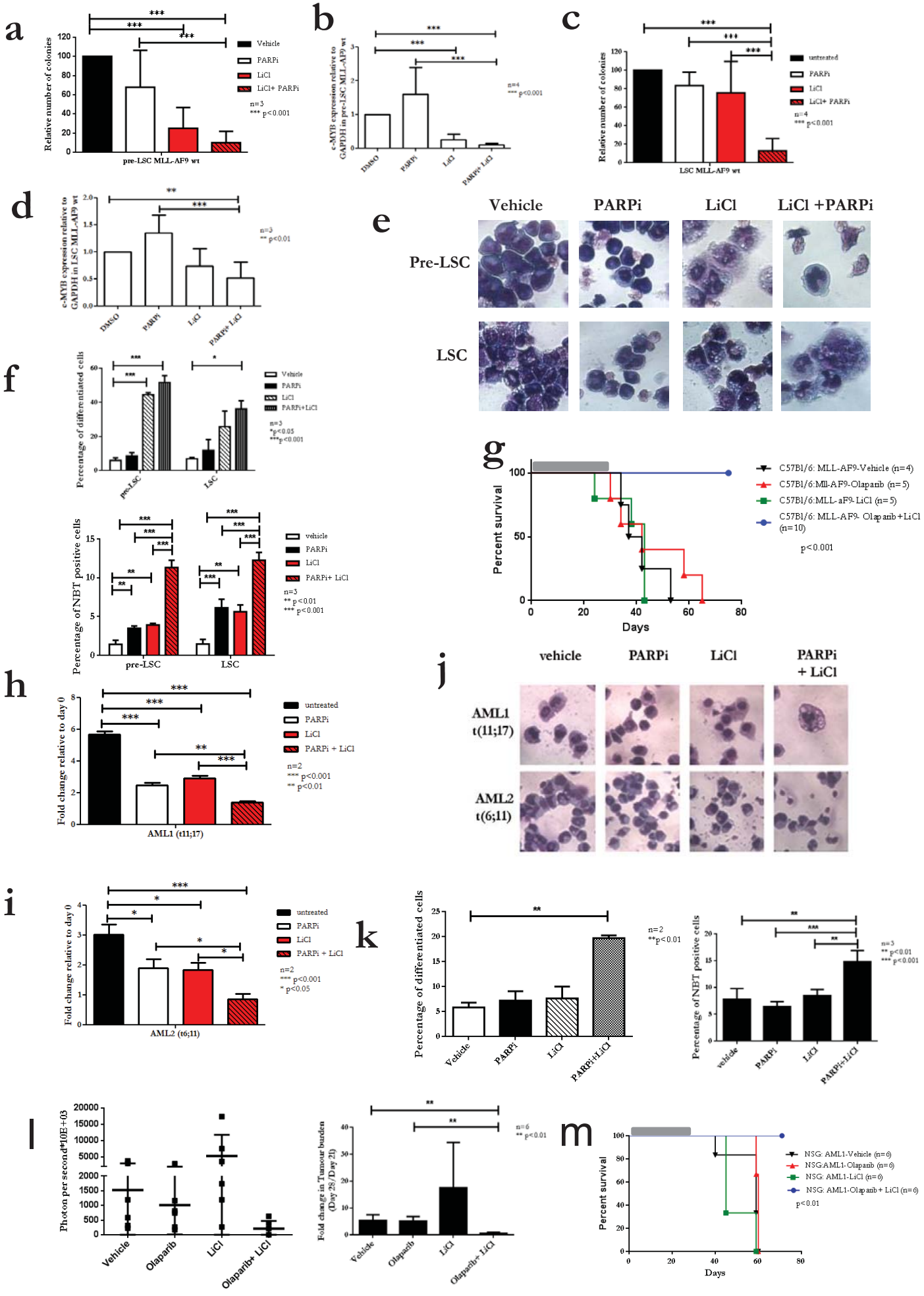
a
Relative number of colonies
Vehicle
PARPi
LiCl
LiCl+ PARPi
n=3
*** p<0.001
pre-LSC MLL-AF9 wt
b
c-MYB expression relative to GAPDH in pre-LSC MLL-AF9 wt
DMSO
PARPi
LiCl
PARPi+ LiCl
n=4
*** p<0.001
c
Relative number of colonies
untreated
PARPi
LiCl
LiCl+ PARPi
n=4
*** p<0.001
LSC MLL-AF9 wt
d
c-MYB expression relative to GAPDH in LSC MLL-AF9 wt
n=3
** p<0.01
e
Vehicle
PARPi
LiCl
LiCl +PARPi
Pre-LSC
LSC
f
Percentage of differentiated cells
Vehicle
PARPi
LiCl
PARPi+LiCl
n=3
*p<0.05
***p<0.001
pre-LSC
LSC
Percentage of NBT positive cells
vehicle
PARPi
LiCl
PARPi+ LiCl
n=3
** p<0.01
*** p<0.001
g
Percent survival
Days
C57Bl/6: MLL-AF9-Vehicle (n=4)
C57Bl/6:Mll-AF9-Olaparib (n=5)
C57Bl/6:MLL-aF9-LiCl (n=5)
C57Bl/6: MLL-AF9- Olaparib+LiCl (n=10)
p<0.001
h
Fold change relative to day 0
untreated
PARPi
LiCl
PARPi + LiCl
n=2
*** p<0.001
** p<0.01
AML1 (t11;17)
j
vehicle
PARPi
LiCl
PARPi + LiCl
AML1 t(11;17)
AML2 t(6;11)
i
Fold change relative to day 0
untreated
PARPi
LiCl
PARPi + LiCl
n=2
*** p<0.001
* p<0.05
AML2 (t6;11)
k
Percentage of differentiated cells
n=2
**p<0.01
Vehicle
PARPi
LiCl
PARPi+LiCl
Percentage of NBT positive cells
n=3
** p<0.01
*** p<0.001
vehicle
PARPi
LiCl
PARPi+LiCl
l
Photon per second*10E+03
Vehicle
Olaparib
LiCl
Olaparib+ LiCl
Fold change in Tumour burden (Day 28/Day 21)
n=6
** p<0.01
Vehicle
Olaparib
LiCl
Olaparib+ LiCl
m
Percent survival
Days
NSG: AML1-Vehicle (n=6)
NSG:AML1-Olaparib (n=6)
NSG: AML1-LiCl (n=6)
NSG: AML1-Olaparib+ LiCl (n=6)
p<0.01

Supplementary Figure 1: data related to Figure 1

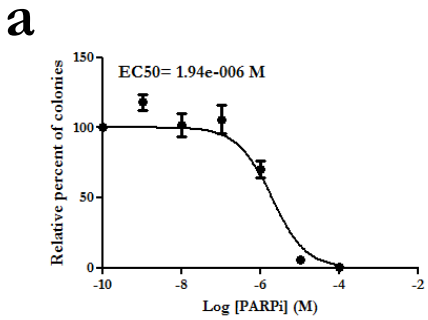

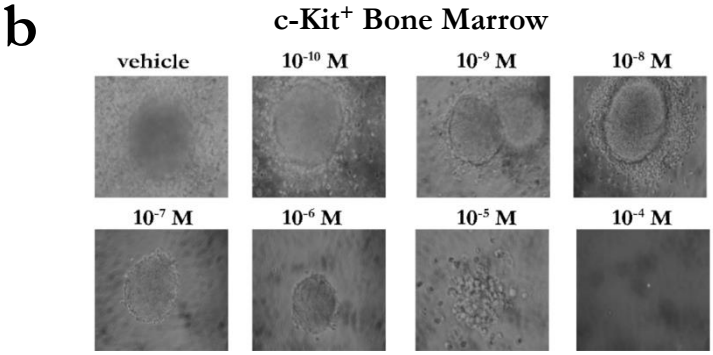

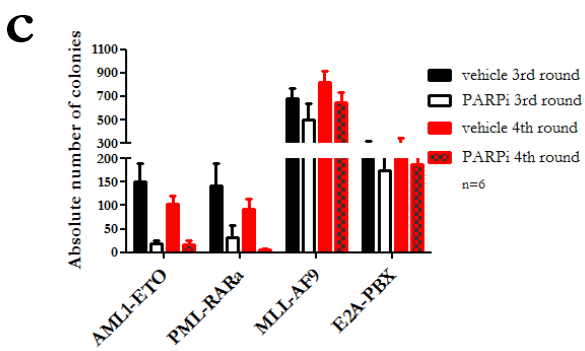

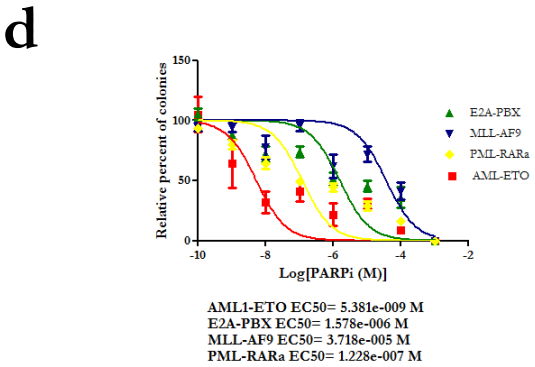

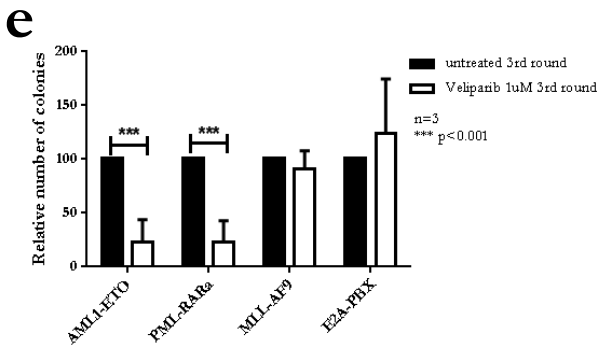

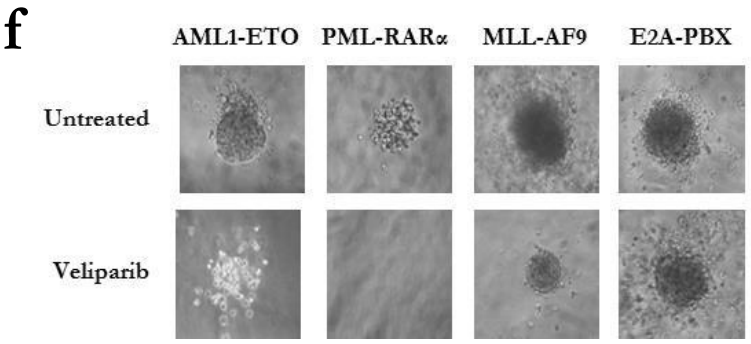

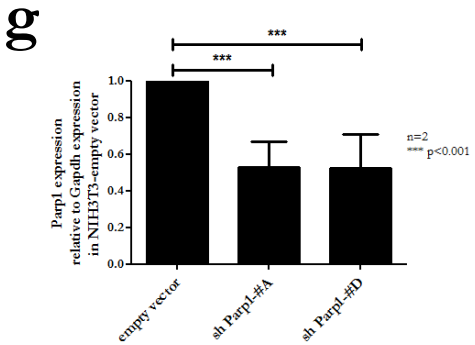

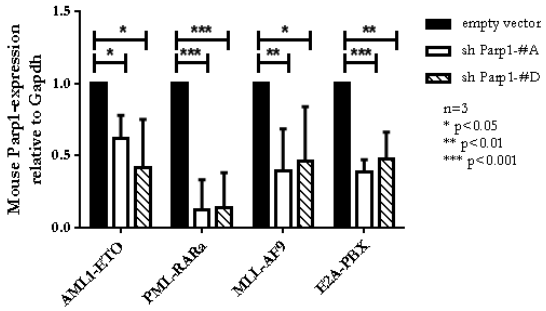

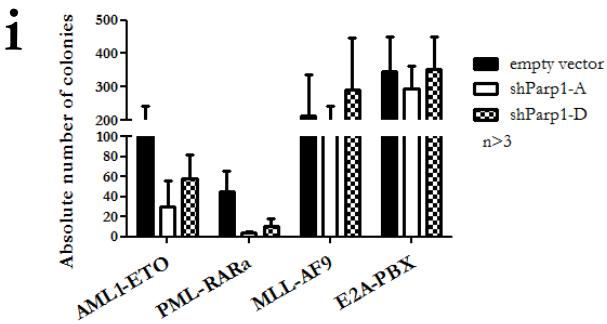

Supplementary Figure 1: data related to Figure 1

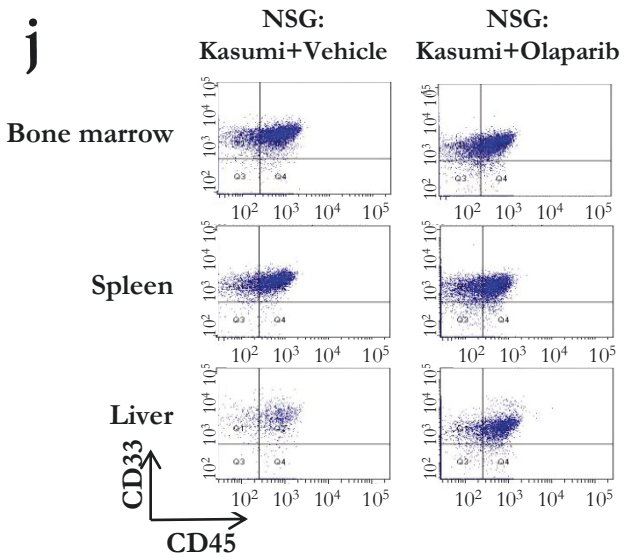

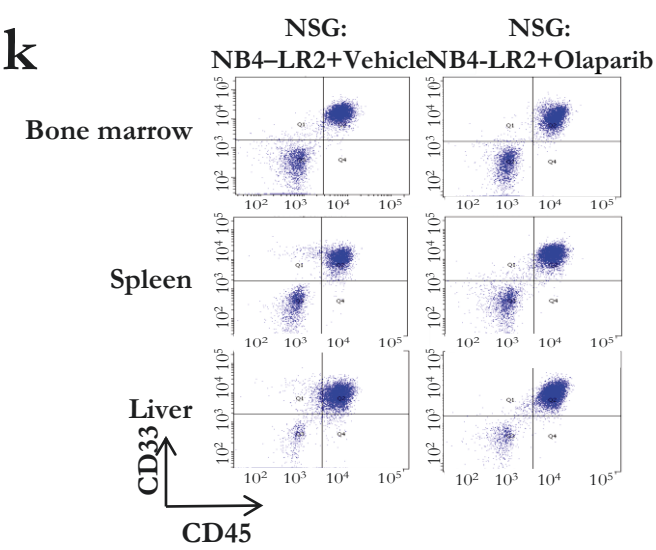

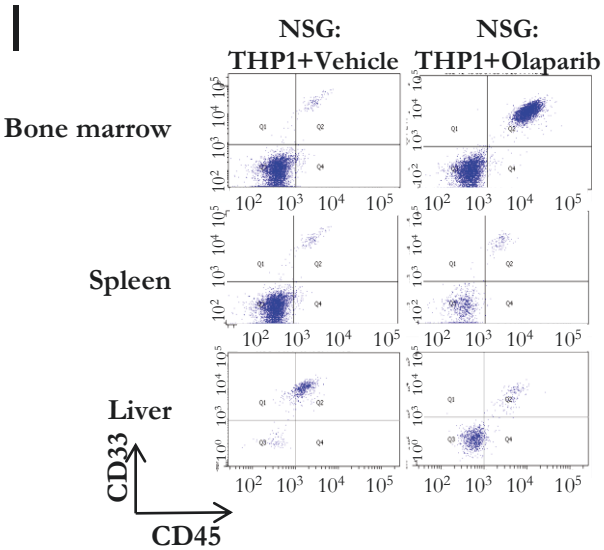

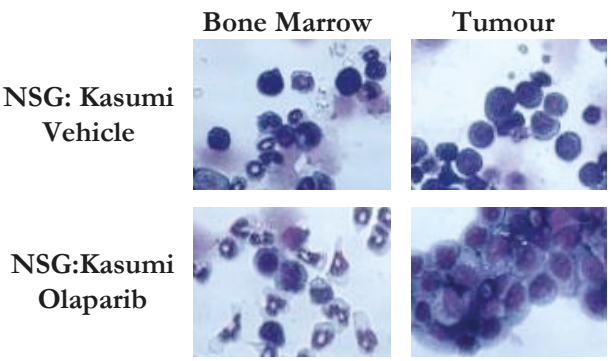

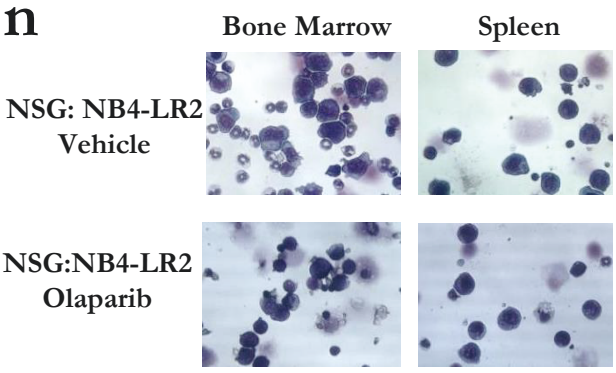

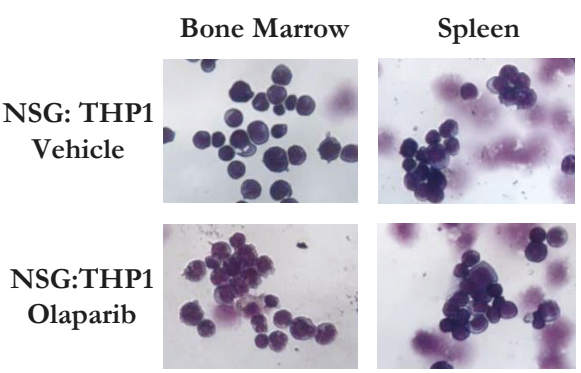

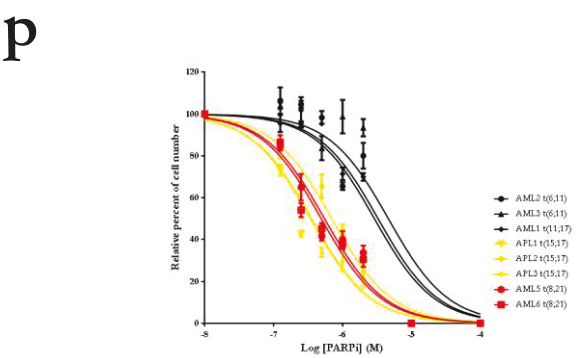

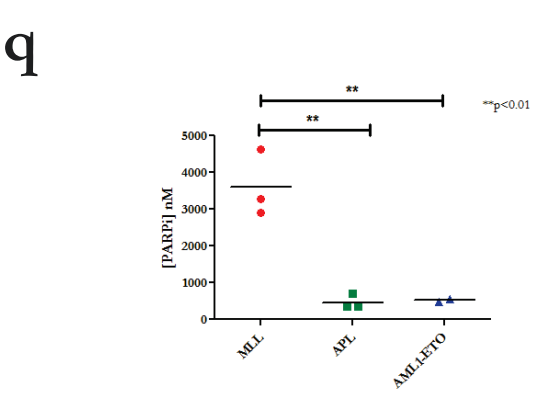

Supplementary Figure 2: data related to Figure 2

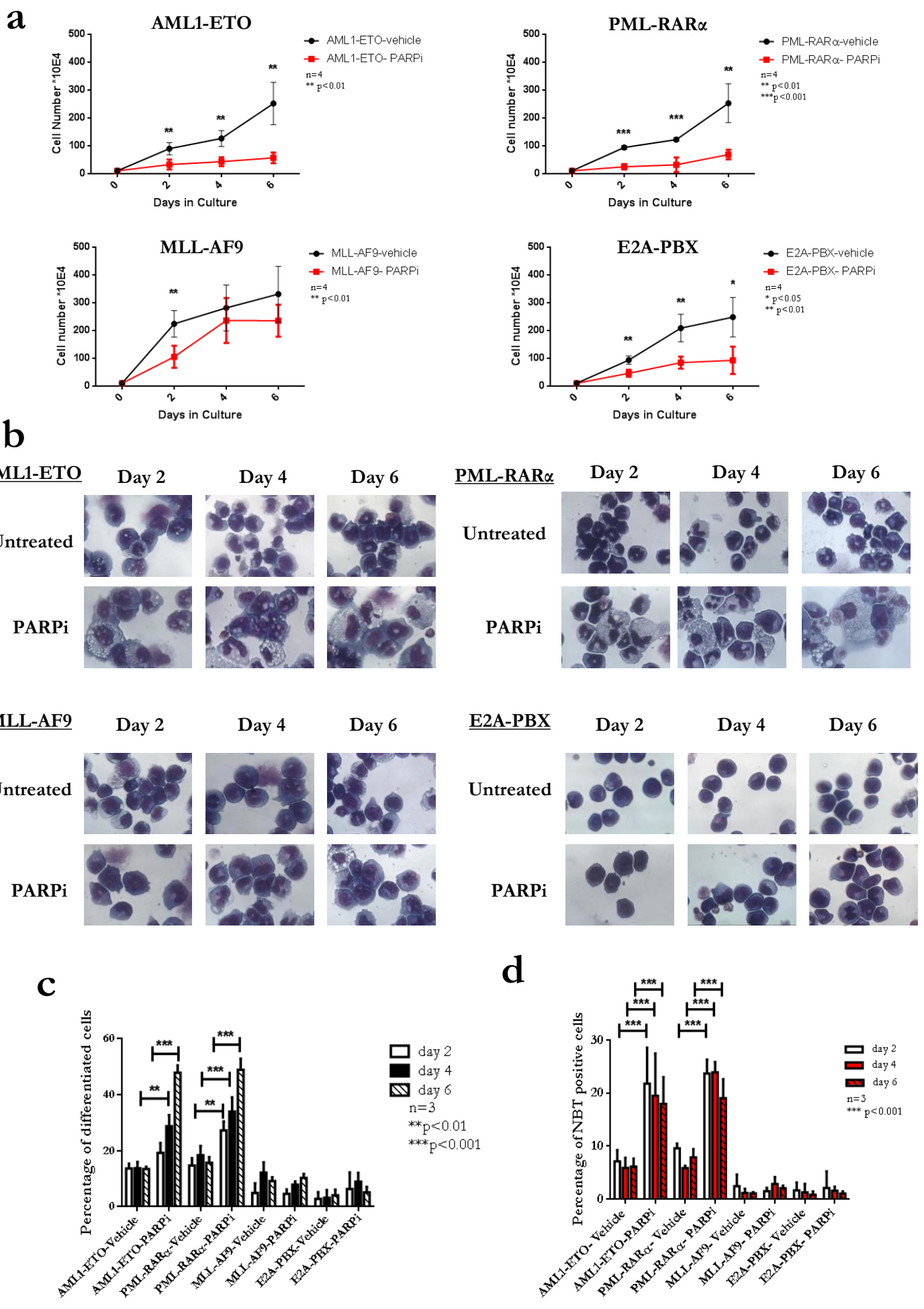

Supplementary Figure 2: data related to Figure 2

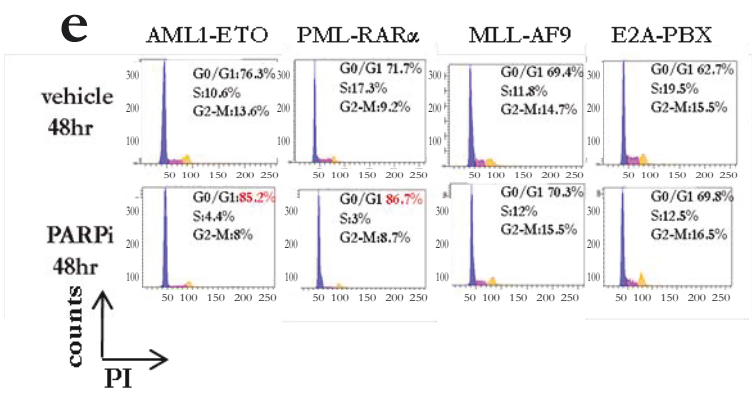

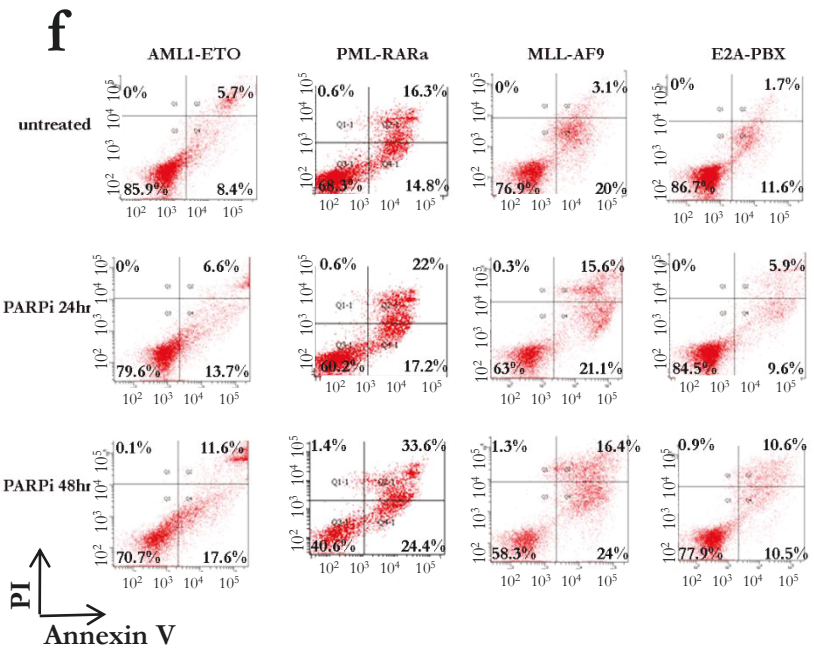

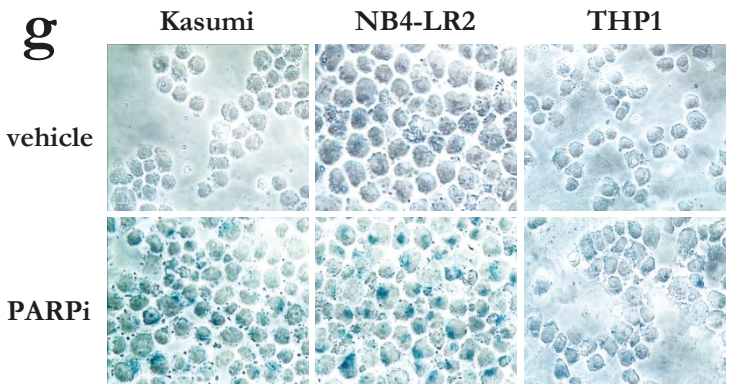

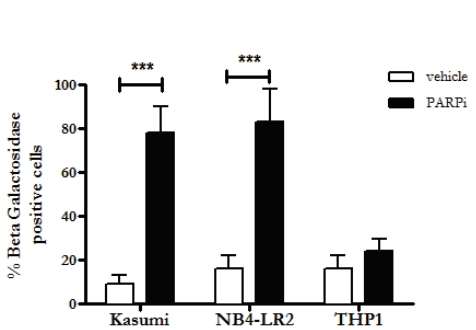

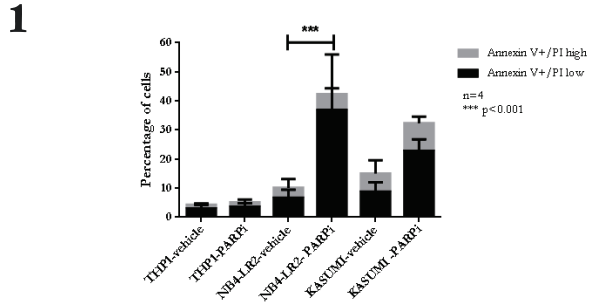

Supplementary Figure 2: data related to Figure 2

j

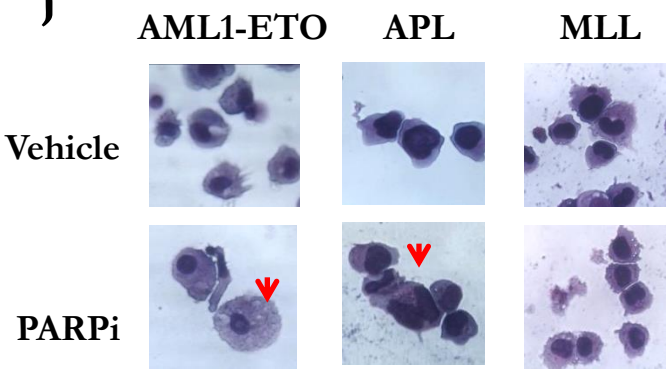

k

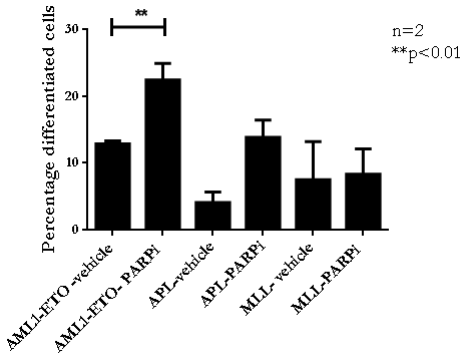

l

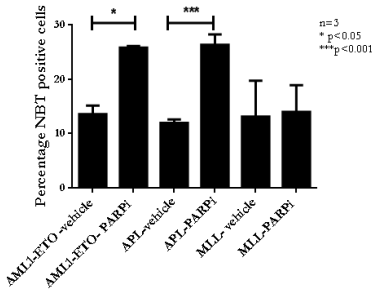

Supplementary Figure 3: data related to Figure 3

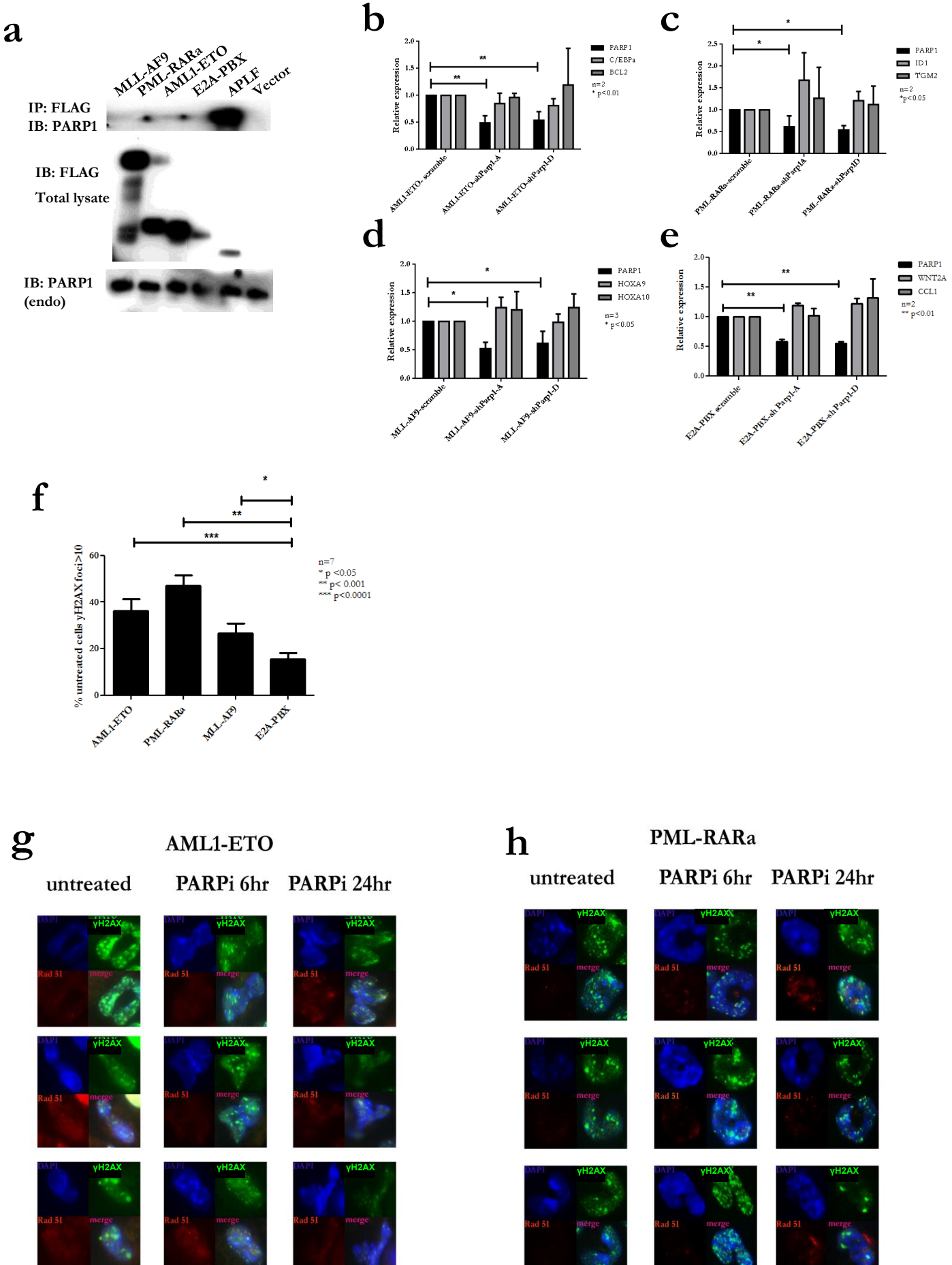

Supplementary Figure 3: data related to Figure 3

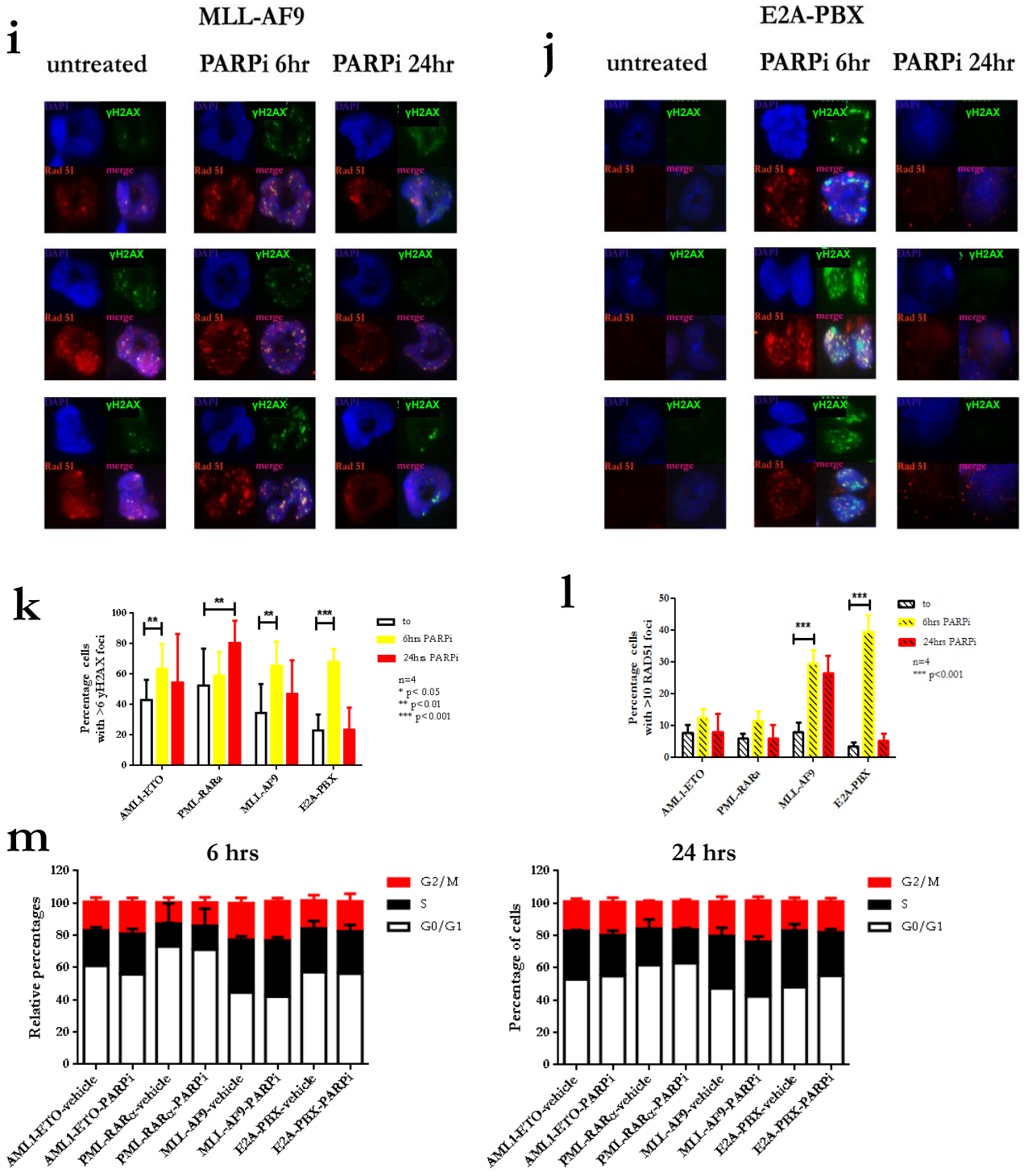

Supplementary Figure 3: data related to Figure 3

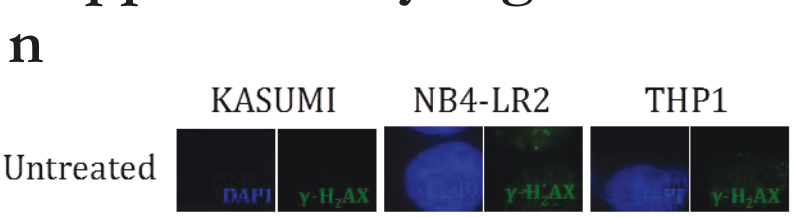

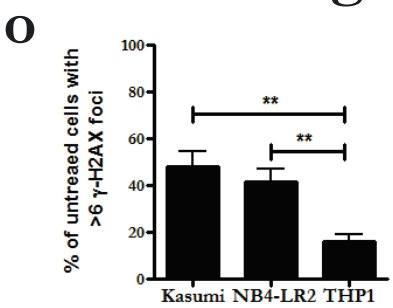

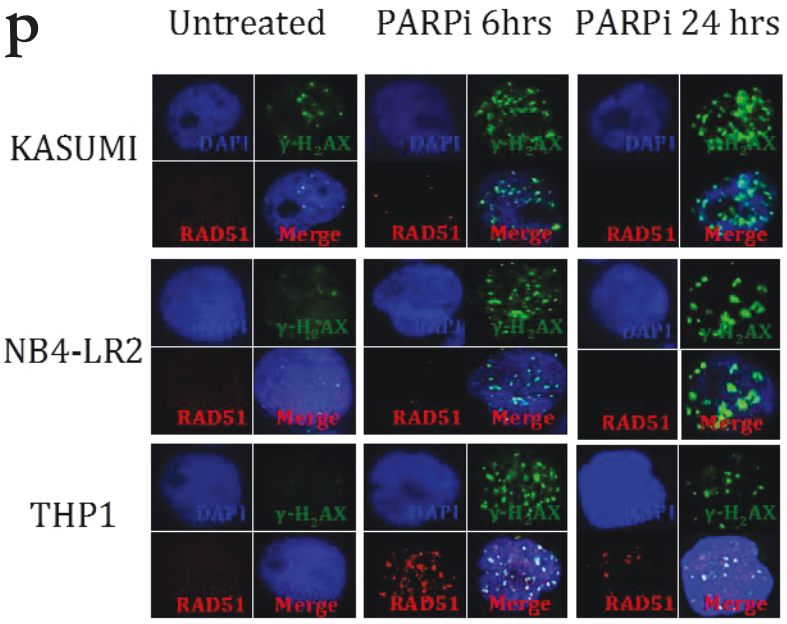

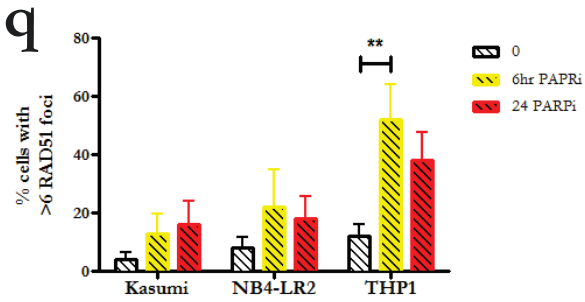

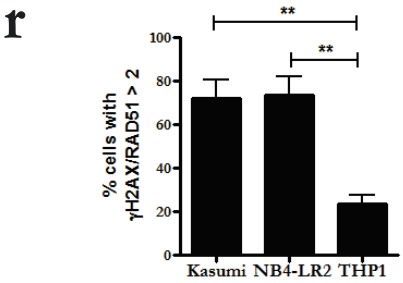

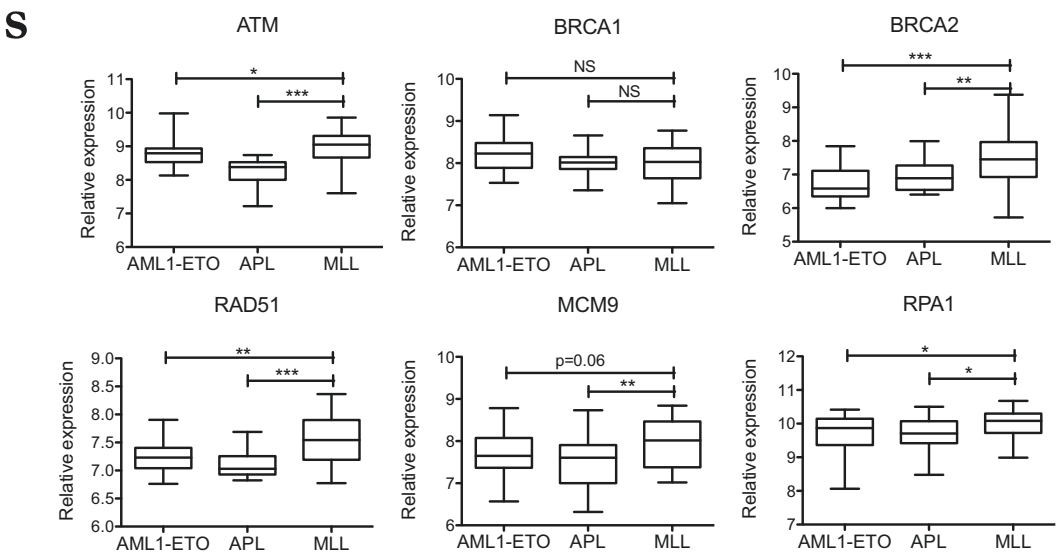

Supplementary Figure 4: data related to Figure 4

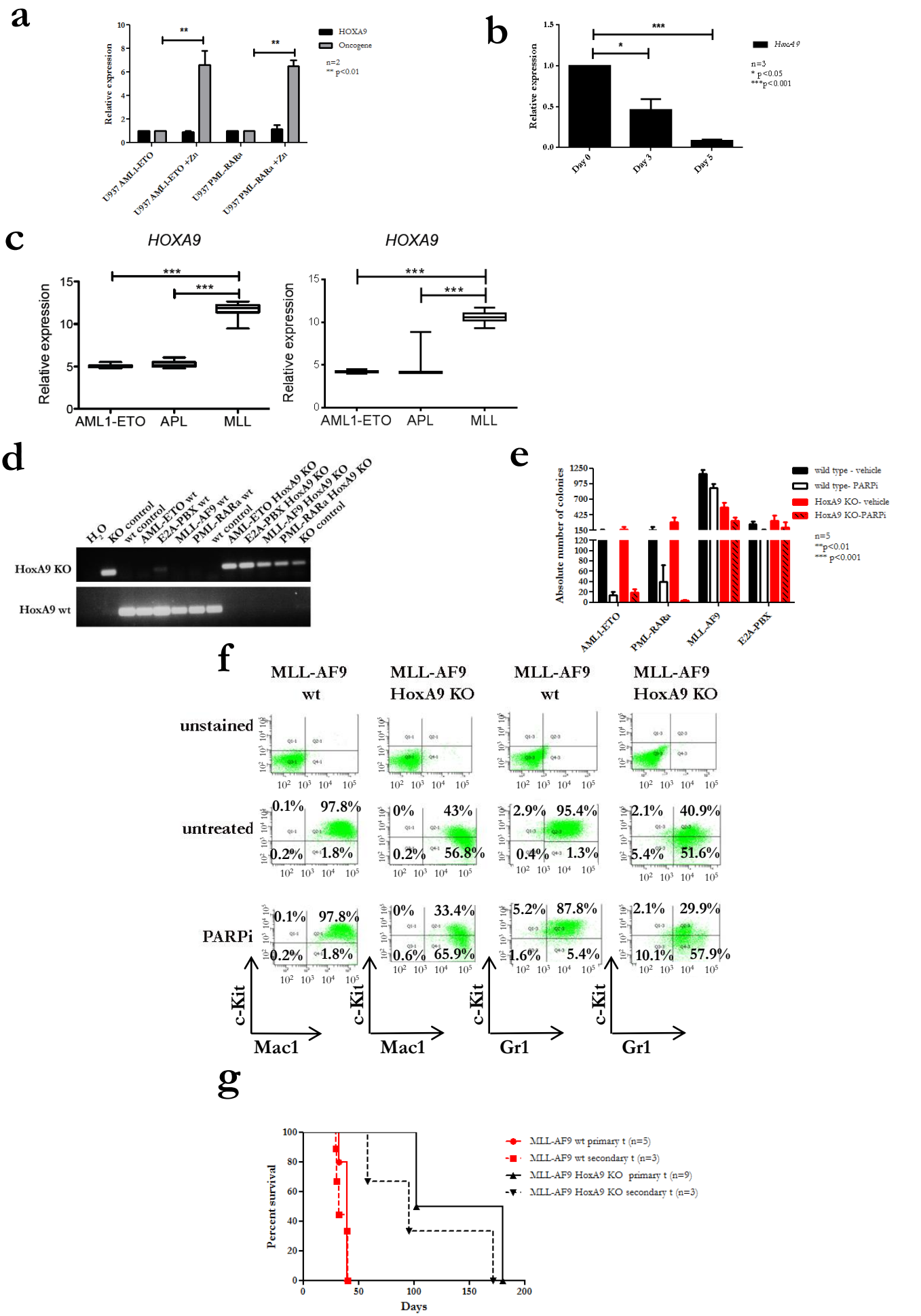

Supplementary Figure 4: data related to Figure 4

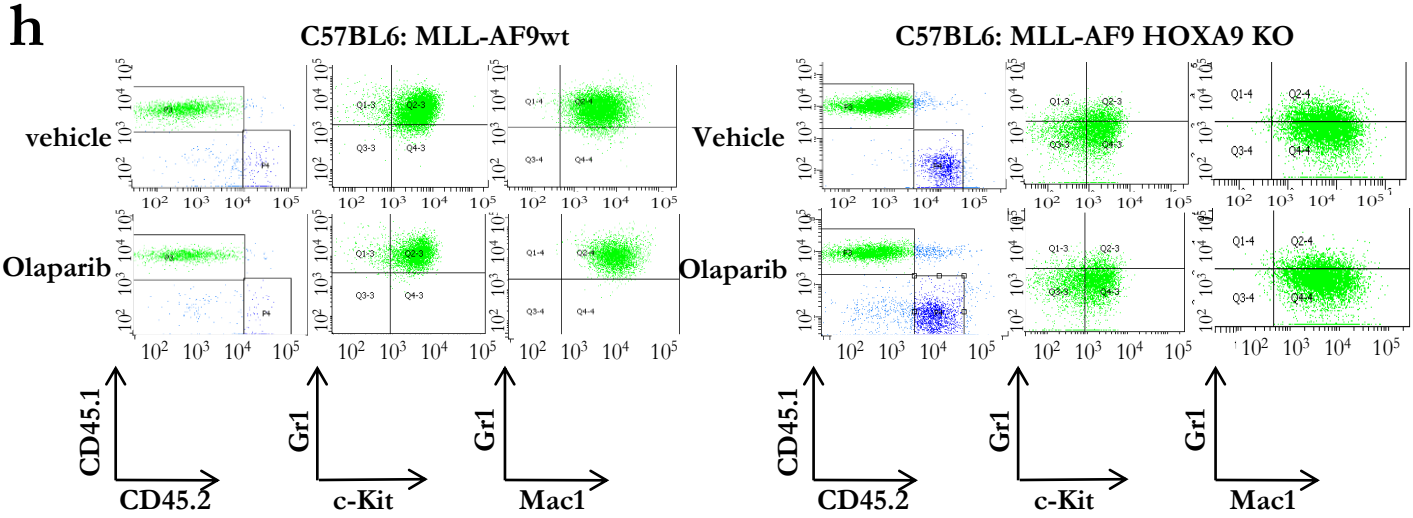

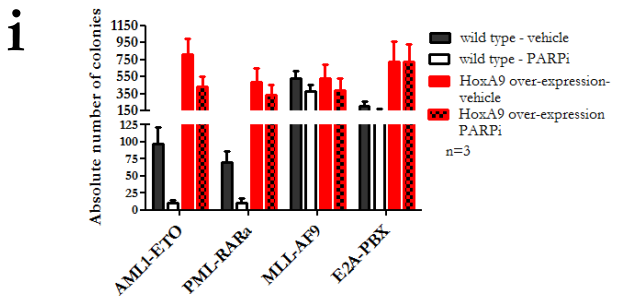

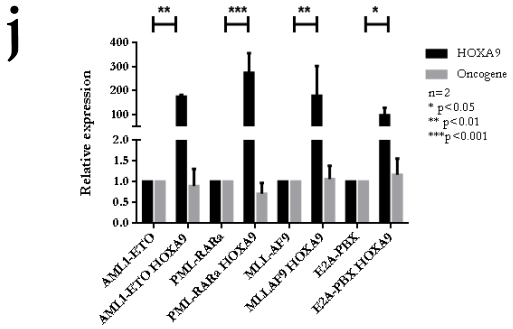

Supplementary Figure 5: data related to Figure 5

a

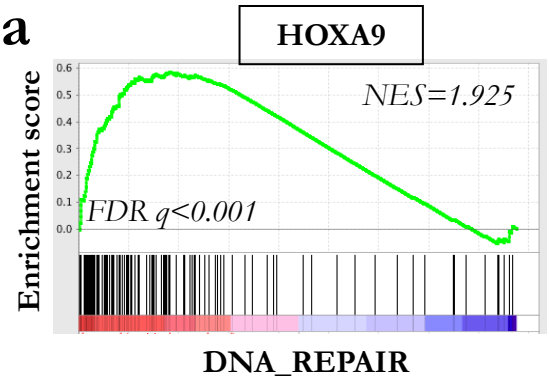

b

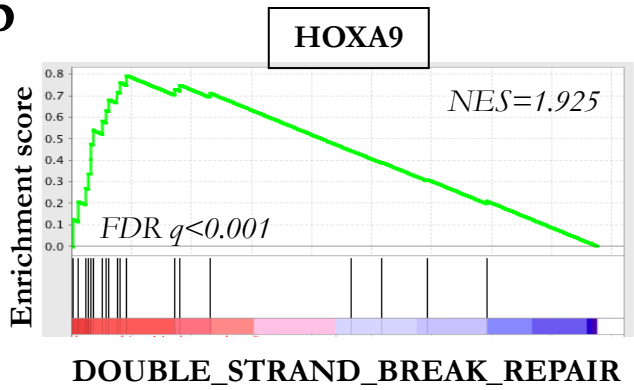

c

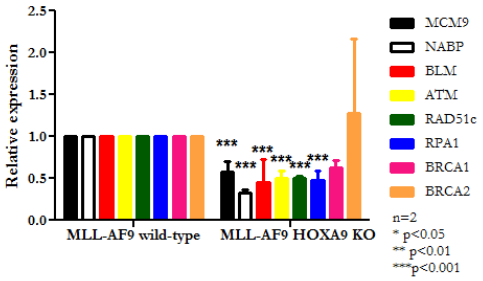

Supplementary Figure 6: data related to Figure 6

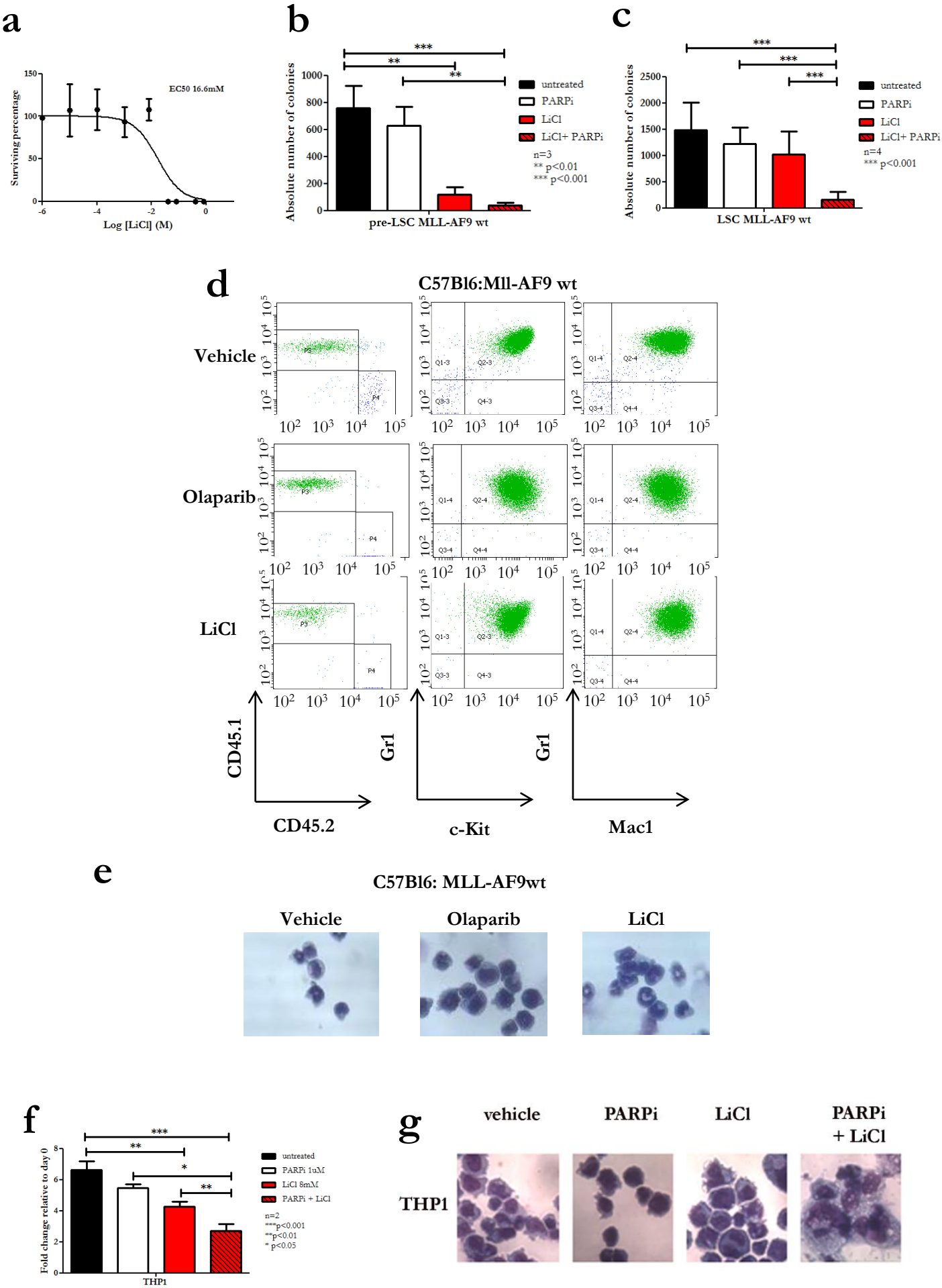

Supplementary Figure 6: data related to Figure 6

h

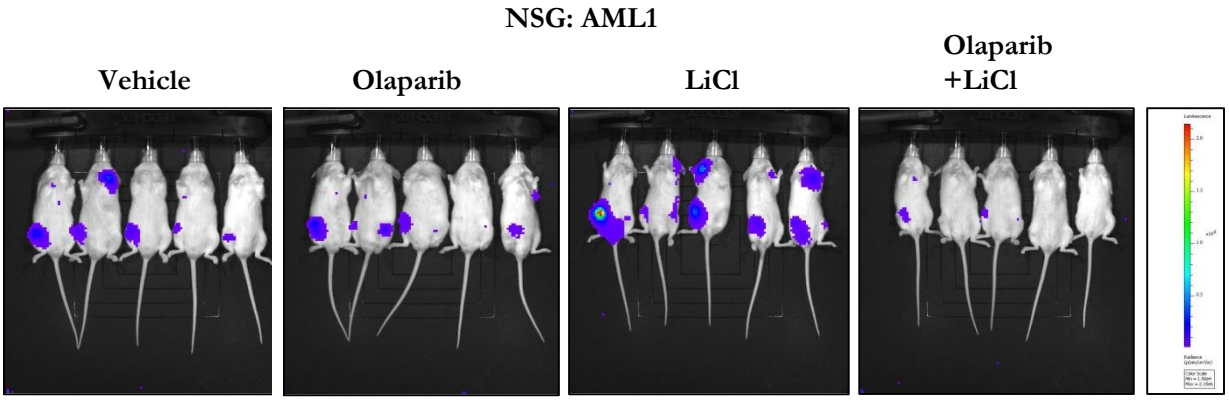

i

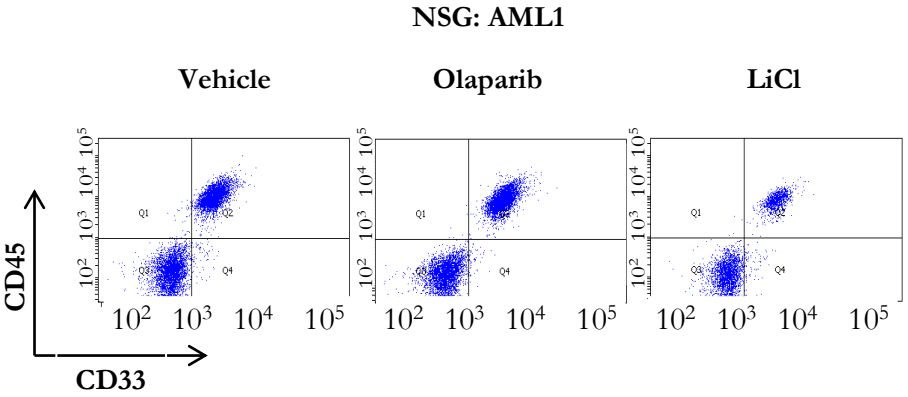

j

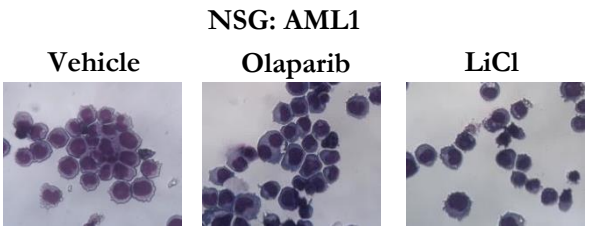

Supplementary Figure 7: Proposed Model

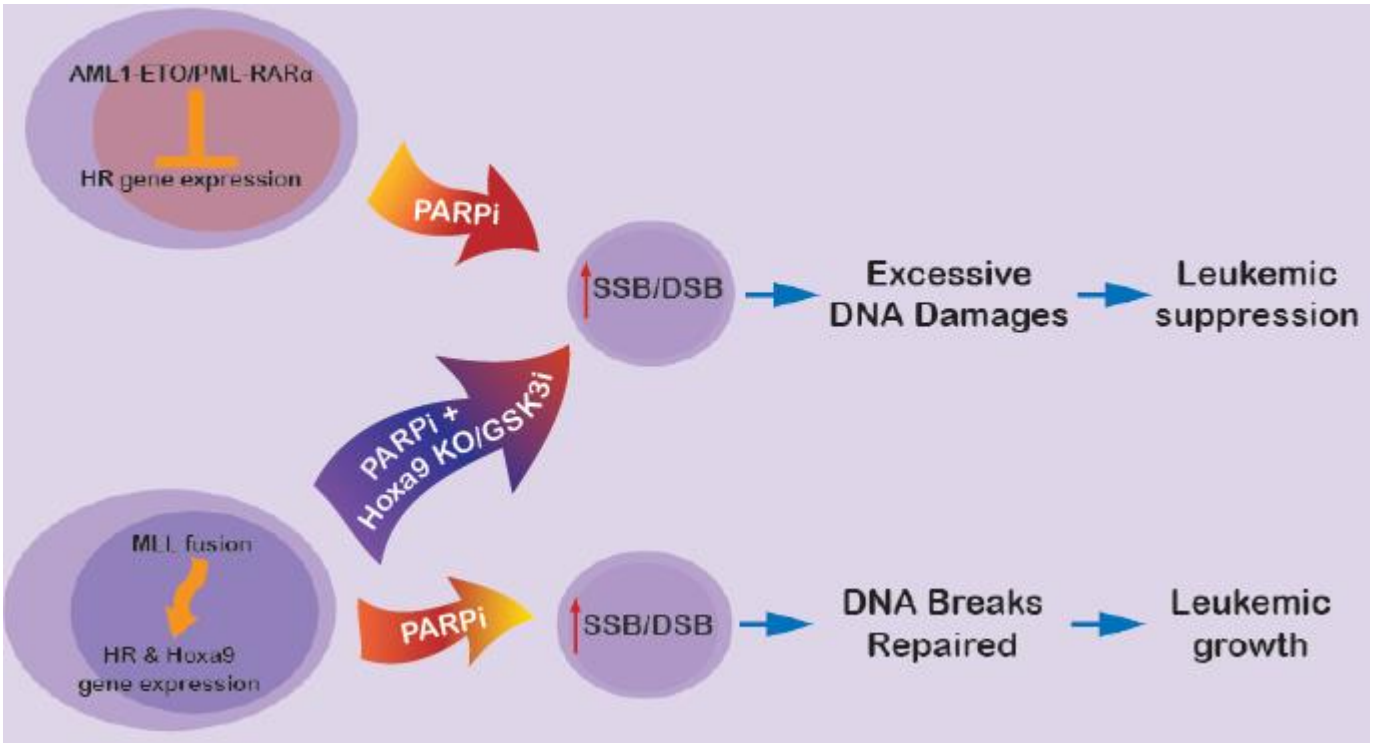

Table S1: Table, related to Figure 1g, summarising the characteristics of NSG mice succumbed with Kasumi driven disease

	Vehicle (n=6)	Olaparib (n=5)	Normal*
Disease Latency (days; median)	55	102	N/A
Spleen (g)	0.0873±0.0409	0.1630±0.1198	0.03997±0.0056
Liver (g)	1.843±0.1330	1.999±0.3720	1.037±0.1050
BM Engraftment (%)	49.22±21.47	41.35±27.73	N/A
Hematopoietic Spleen Engraftment (%)	39.84±21.93	48.68±33.71	N/A
Hematopoietic Liver Engraftment (%)	42.76±30.9	41.68±26.19	N/A
CBC WBC (10^9/L)	2.5± 0.8485	2.9± 2.832	5.238±3.763
CBC RBC (10^{12}/L)	6.68±0.396	6.835±1.328	7.235±0.8716
CBC Platelets (10^9/L)	349±39.6	514.8±245.2	467.9±231.7

N/A: not applicable

* Normal: normal NSG mice. Data collected from 3 animals

Table S2: Table, relating to Figure 1h, summarising the characteristics of NSG mice succumbed with NB4-LR2 driven disease

	Vehicle (n=5)	Olaparib (n=10)	Normal*
Disease Latency (days; median)	39	51	N/A
Spleen (g)	0.1216±0.0232	0.5226±0.5279	0.03997±0.0056
Liver (g)	2.26±0.401	2.415±1.844	1.037±0.1050
BM Engraftment (%)	30.94±23.11	40.27±23.73	N/A
Hematopoietic Spleen Engraftment (%)	22.8±25.13	33.39±25.3	N/A
Hematopoietic Liver Engraftment (%)	47.64±19.68	58.99±27.07	N/A
CBC WBC (10^9/L)	3.875± 3.288	2.322± 1.177	5.238±3.763
CBC RBC (10^{12}/L)	8.14±3.857	7.576±3.309	7.235±0.8716
CBC Platelets (10^9/L)	442.3±177.9	406.3±43.46	467.9±231.7

N/A: not applicable

* Normal: normal NSG mice. Data collected from 3 animals.

Table S3: Table, relating to Figure 1i, summarising the characteristics of NSG mice succumbed with THP1 driven disease

	Vehicle (n=6)	Olaparib (n=6)	Normal
Disease Latency (days; median)	81	81	N/A
Spleen (g)	0.108±0.0146	0.0822±0.0301	0.03997±0.0056
Liver (g)	1.28±0.147	1.31±0.153	1.037±0.1050
BM Engraftment (%)	3.266±2.153	30.7±33.27	N/A
Hematopoietic Spleen Engraftment (%)	8.831±5.679	8.53±6.946	N/A
Hematopoietic Liver Engraftment (%)	46.48±43.05	27.81±31.79	N/A
CBC WBC (10^9/L)	4.1±3.69	6.18±4.22	5.238±3.763
CBC RBC (10^{12}/L)	7.653±0.611	8.526±1.575	7.235±0.8716
CBC Platelets (10^9/L)	183.83±70.25	132.2±27.58	467.9±231.7

N/A: not applicable

* Normal: normal NSG mice. Data collected from 3 animals.

Table S4: Genes associated with GO:0000724: double-strand break repair via homologous recombination analysis enriched in gene ontology (GO) analysis of gene expression in human leukemia with MLL-rearrangement compared to APL and AML1-ETO subtypes (column 1) and HOXA9 responsive genes (column 2) in published datasets. Highlighted are DDR genes commonly activated by MLL fusions and Hoxa9.

MLL-rearrangement	HOXA9
RAD51	**RAD51**
MCM9	MCM9
ATM	ATM
BLM	BLM
BRCA1	BRCA1
BRCA2	BRCA2
CHEK1	CHEK1
HUS1	HUS1
MRE11A	MRE11A
PARPBP	PARPBP
RAD51C	RAD51C
RPA1	RPA1
RAD50	ERCC4
MORF4L1	NABP2
TERF2IP	PPP4C
NBN	RAD21L1
H2AFX	RAD51B
NABP2	RAD51D
RBBP8	RAD52
MDC1	RAD54B
RAD51AP1	RTEL1
PSMD14	SIRT6
PALB2	SMC6
RPA2	TEX15
LIG1	TONSL
RPA3	XRCC3
SHFM1	
SMC5	
UBE2N	
YY1	

Table S5 Table, relating to Figure 4f, summarising the characteristics of C57bl6 mice succumbed with MLL-AF9 wild-type driven leukemia

	Vehicle (n=12)	Olaparib (n=12)	Normal*
Disease Latency (days; median)	31	34	N/A
Spleen (g)	0.7968±0.39	0.9309±0.3767	0.1130±0.03430
Liver (g)	3.486±1.71	4.204±1.425	1.331±0.2650
BM Engraftment (%)	95.99±5.054	93.30±9.257	N/A
Hematopoietic Spleen Engraftment (%)	90.25±8.872	86.85±13.12	N/A
Hematopoietic Liver Engraftment (%)	94.22±3.393	93.16±6.838	N/A
CBC WBC (10^9/L)	26.87±35.61	26.03±34.48	19.32±3.177
CBC RBC (10^{12}/L)	5.573±0.7508	5.735±3.426	8.620±0.3385
CBC Platelets (10^9/L)	190±68.02	203±255.1	357.8±83.54

N/A: not applicable

* Normal C57Bl6 mice: Data collected from 3 mice

Table S6: Table relating to Figure 4g, summarising the characteristics of C57Bl6 mice succumbed with MLL-AF9-Hoxa9 KO driven leukemia

	Vehicle (n=14)	Olaparib (n=11)	Normal*
Disease Latency (days; median)	32	67	N/A
Spleen (g)	0.5429±0.1810	0.4337±0.1559	0.1130±0.03430
Liver (g)	2.127±0.5528	1.696±0.1262	1.331±0.2650
BM Engraftment (%)	61.3±28.64	82.06±18.95	N/A
Hematopoietic Spleen Engraftment (%)	50.62±33.78	65.4±33.45	N/A
Hematopoietic Liver Engraftment (%)	64.02±23.34	62.18±38.26	N/A
CBC WBC (10^9/L)	41.4±47.8	53.93±51.06	19.32±3.177
CBC RBC (10^{12}/L)	5.187±1.95	4.153±2.066	8.620±0.3385
CBC Platelets (10^9/L)	223±83.45	227±166	357.8±83.54

N/A: not applicable

* Normal C57Bl6 mice: Data collected from 3 mice

Table S7: Table, relating to Figure 6g, summarising the characteristics of C57Bl6 mice succumbed with MLL-AF9 wild-type driven leukemia.

	Vehicle (n=4)	Olaparib (n=5	LiCl (n=5)	Olaparib+LiCl (n=10)	Normal*
Disease Latency (days; mean)	41.5	45.8	38.2	N/A**	N/A
Spleen (g)	1.115±0.3960	1.218±0.3266	1.108±0.4018	N/A	0.1130±0.03430
Liver (g)	2.483±0.4211	2.868±0.4089	2.625±0.6598	N/A	1.331±0.2650
BM Engraftment (%)	95.03±2.2937	80.23±23.70	97.23±1.408	N/A	N/A
Hematopoietic Spleen Engraftment (%)	86.47±3.523	65.07±43.46	91.28±4.623	N/A	N/A
Hematopoietic Liver Engraftment (%)	92.97±3.175	76.5±19.21	93.73±5.5508	N/A	N/A
CBC WBC (10^9/L)	26.87±35.61	26.03±34.48	24.03±28.11	N/A	19.32±3.177
CBC RBC (10^{12}/L)	5.573±0.7508	5.735±3.426	5.29±2.578	N/A	8.620±0.3385
CBC Platelets (10^9/L)	190±68.02	203±255.1	135.8±89.68	N/A	357.8±83.54

N/A: not applicable

* Normal C57Bl6 mice: Data collected from 5 mice

** No disease latency because no animal comes down with disease.

Table S8: Table, relating to figure 6m, summarising the characteristics of NSG mice succumbed to leukemia driven by primary AML1 cells treated with Olaparib, Li diet or combination therapy in vivo.

	Vehicle (n=6)	Olaparib (n=6)	Li diet (n=6)	Olaparib+Li diet (n=6)	Normal*
Disease Latency (days; median)	59	60	45	N/A**	N/A
Spleen (g)	0.076±0.030	0.136±0.029	0.133±0.060	N/A	0.03997±0.0056
Liver (g)	1.20±0.157	1.30±0.134	1.27±0.091	N/A	1.037±0.1050
BM Engraftment (%)	57.98±30.49	53.23±23.21	28.72±15.19	N/A	N/A
Hematopoietic Spleen Engraftment (%)	11.30±7.885	2.733±4.166	1.760±3.266	N/A	N/A
Hematopoietic Liver Engraftment (%)	42.65±22.61	23.20±20.61	16.93±17.75	N/A	N/A
CBC WBC (10^9/L)	3.000±2.160	3.950±3.265	5.267±7.450	N/A	5.238±3.763
CBC RBC (10^{12}/L)	7.978±0.659	6.652±1.908	5.960±2.003	N/A	7.235±0.8716
CBC Platelets (10^9/L)	307.8±160.9	393.2±293.6	314.3±274.1	N/A	467.9±231.7

N/A: not applicable

* Normal NSG mice: Data collected from 6 mice

** No disease latency and engraftment data because no animal comes down with disease.

Table S9: List of antibodies (The antibodies provided as gift were mentioned in materials and methods).

Antibody	Supplier	Catalog number	Application	Dilution
Actin-HRP	Scbt	Sc-1616	Western Blot	1:1000
Phospho-y H2AX (ser139)	Upstate	05-636	Immunofluorescence	1:200
Rad51	Scbt	Sc-8349	Western Blot	1:500
Rad51	Scbt	Sc-8349	Immunofluorescence	1:100
PARP1	Cell signaling	#9542S	Western Blot	1:1000
FLAG (M2)	Sigma	F1804	Western Blot Immunoprecipitation	1:5000 1ug

Table S10. List of Primers sequences*

Primer	Sequence	Application
mouse Rad51 F	aagttttggtccacagcctattt	qRT-PCR
mouse Rad51 R	cggtgcataagcaacagcc	qRT-PCR
mouse p53 F	ctctcccccgcaaaagaaaaa	qRT-PCR
mouse p53 R	cggaacatctcgaagcgttta	qRT-PCR
mouse p21 F	ccacagcgatatccagacattc	qRT-PCR
mouse p21 R	gcggaacaggtcggacat	qRT-PCR
mouse Xrcc2 F	ggaaaggcccacatgtgagt	qRT-PCR
mouse Xrcc2 R	ggatcgtttgtgacataggcatt	qRT-PCR
mouse Parp1 F	gctttatcgagtggagtacgc	qRT-PCR
mouse Parp1 R	ggagggagtccttgggaatac	qRT-PCR
mouse Gapdh F	gtatgactccactcacggcaaa	qRT-PCR
mouse Gapdh R	ttcccattctcggccttg	qRT-PCR
mouse Brca1 F	aagagacagtaactaagccaggt	qRT-PCR
mouse Brca1 R	ggggcggtctgtaacaattcc	qRT-PCR
mouse Brca2 F	atgcccgttgaatacaaaagga	qRT-PCR
mouse Brca2 R	accgtggggcttatactcaga	qRT-PCR
mouse c-Myb F	agaccccgacacagcatcta	qRT-PCR
mouse c-Myb R	ccgggccgaagagatttctg	qRT-PCR
human HOXA9 F	gccggccttatggcattaa	qRT-PCR (Taqman)
human HOXA9 R	cagggacaaagtgtgagtgtcaa	qRT-PCR (Taqman)
human HOXA9 probe	FAM-tgaaccgctgtcggccagaagg-TAMRA	qRT-PCR(Taqman)
mouse HoxA9 F	ccgaacaccccgacttca	qRT-PCR (Taqman)
mouse HoxA9 R	ttccacgaggcaccaaaca	qRT-PCR (Taqman)
mouse HoxA9 probe	FAM-tgcagcttccagtccaaggcgg-TAMRA	qRT-PCR (Taqman)
mouse Gapdh Taqman primers and probe	Applied Biosystem #4331182	qRT-PCR (Taqman)
human GAPDH Taqman primers and probe	Applied Biosystem #402869	qRT-PCR (Taqman)
mouse p16F	cgtgagggcactgctggaag	qRT-PCR
mouse p16R	accagcgtgtccaggaagcc	qRT-PCR
mouse Mcm9F	ggtcaggtgtttgagtcctatg	qRT-PCR
mouse Mcm9R	ggtcaggtgtttgagtcctatg	qRT-PCR
Mouse AtmF	ccagctttttgatgcagatacca	qRT-PCR
Mouse AtmR	ccagctttttgatgcagatacca	qRT-PCR
Mouse Rpa1F	acatccgtcccatttctacagg	qRT-PCR
Mouse Rpa1R	ctccctcgaccagggtgtt	qRT-PCR
mouse HoxA9 wt F	cacaaaggggctctaaatcc	Genotype PCR
mouse HoxA9 wt R	agcacatacagccaatagcg	Genotype PCR
mouse HoxA9 KO F	aaggcaggtcaagatctccga	Genotype PCR
mouse HoxA9 KO R	tcgccttcttgacgagttctt	Genotype PCR
Mouse Bcl2 F	ggggtcatgtgtgtggagag	qRT-PCR
Mouse Bcl2 R	gcatgctggggccatatagt	qRT-PCR
Mouse Tgm2 F	agagtgtcgtctcctgctct	qRT-PCR
Mouse Tgm2 R	gtagggatccagggtcaggt	qRT-PCR
Mouse Id1 F	gagtctgaagtcgggaccac	qRT-PCR
mouse Id1 R	ctggaacacatgccgcct	qRT-PCR
mouse Wnt16 F	ccagtacggcatgtggttca	qRT-PCR
mouse Wnt16 R	gacattaacttggcgacagcc	qRT-PCR
Mouse Ccl1 F	gcaagagcatgcttacggtc	qRT-PCR
Mouse Ccl1 R	tagttgaggcgcagctttct	qRT-PCR

* qRT-PCR primers are for SYBR-Green except those mentioned (Taqman). Genotype PCR were performed by conventional PCR.